

# Experimental investigations on growth of GaN-based materials for light emitting applications

---

Muhammad Ali



# Experimental investigations on growth of GaN-based materials for light emitting applications

**Muhammad Ali**

Doctoral dissertation for the degree of Doctor of Science in  
Technology to be presented with due permission of the School of  
Electrical Engineering for public examination and debate in TUAS  
building (auditorium AS1) at the Aalto University School of Electrical  
Engineering (Espoo, Finland) on the 16th of November 2012 at 12  
noon

**Aalto University**  
**School of Electrical Engineering**  
**Department of Micro- and Nanosciences**  
**Optoelectronics group**

**Supervising professor**

Professor Markku Sopanen

**Thesis advisor**

Dr. Tech. Sami Suihkonen

**Preliminary examiners**

Professor Arnab Bhattacharyya, Department of Condensed Matter Physics, No.1, Homi Bhabha Road, Tata Institute of Fundamental Research, Mumbai 400 005, India

Dr. Ian Watson, GaN Materials and Devices, Institute of Photonics, University of Strathclyde, Wolfson Centre, 106 Rottenrow, Glasgow G4 0NW, United Kingdom

**Opponent**

Professor Paul (Paulus) Robertus Hageman, Radboud University, Netherlands

Aalto University publication series

**DOCTORAL DISSERTATIONS** 143/2012

© Muhammad Ali

ISBN 978-952-60-4845-1 (printed)

ISBN 978-952-60-4846-8 (pdf)

ISSN-L 1799-4934

ISSN 1799-4934 (printed)

ISSN 1799-4942 (pdf)

<http://urn.fi/URN:ISBN:978-952-60-4846-8>

Unigrafia Oy

Helsinki 2012

Finland



441 697  
Printed matter

**Author**

Muhammad Ali

**Name of the doctoral dissertation**

Experimental investigations on growth of GaN-based materials for light emitting applications

**Publisher** School of Electrical Engineering

**Unit** Department of Micro- and Nanosciences

**Series** Aalto University publication series DOCTORAL DISSERTATIONS 0/2012

**Field of research** Optoelectronics

**Manuscript submitted** 15 May 2012

**Date of the defence** 16 November 2012

**Permission to publish granted (date)** 23 August 2012

**Language** English

☐ **Monograph**

☒ **Article dissertation (summary + original articles)**

**Abstract**

This work investigates the fabrication, characterization and application of GaN-based layers in light emitting structures. All the thin films and light emitting diodes (LEDs) discussed in this thesis were grown by metal organic vapor phase epitaxy (MOVPE). The objective of this thesis was to improve the material quality and light extraction of III-N optoelectronic structures. Scanning electron microscopy (SEM), transmission electron microscopy (TEM), x-ray diffraction (XRD), photoluminescence (PL) and electroluminescence (EL) were used to characterize the samples.

GaN layers were grown on GaN templates having hexagon shaped openings. Embedded voids were created at the GaN-sapphire interface with a novel process described in this work. A control over the shape of the voids was demonstrated. It was observed that changing the diameter of the hexagonal openings has an impact on the inclination angle of the sidewalls of embedded voids. The GaN layers having the embedded voids with low inclination angle sidewalls showed an improved material quality. Significant threading dislocation (TD) bending was observed near such voids. InGaN/GaN LEDs were grown on GaN layers with embedded voids of different shapes. Improved material quality and more efficient light extraction due to the introduced void geometry enhanced the light output of 60 degrees inclined sidewall embedded void LEDs. Light extraction enhancement was also studied by mask-less chemical roughening of the back side of the sapphire substrate. An optimized roughening process improved the light extraction from the LED structure by more than 20 %.

The compositional dependence of indium and aluminum on MOVPE growth conditions in quaternary InAlGa layers was investigated. InGaN multi-quantum well structures (MQWs) having quaternary barriers with near-UV emission were also studied. It was observed that the internal quantum efficiency (IQE) of InGaN/InAlGa MQW structure was sensitive to the barrier layer composition.

A proof-of-concept LED based augmented reality application was demonstrated. A working InGaN/GaN single micro-pixel light source was integrated into a contact lens. The LED micropixel display was controlled via a radio frequency transmitter in free space and tested on a rabbit.

**Keywords** LED, III-nitrides, MOVPE, light extraction, augmented reality

**ISBN (printed)** 978-952-60-4845-1

**ISBN (pdf)** 978-952-60-4846-8

**ISSN-L** 1799-4934

**ISSN (printed)** 1799-4934

**ISSN (pdf)** 1799-4942

**Location of publisher** Espoo

**Location of printing** Helsinki

**Year** 2012

**Pages** 141

**urn** <http://urn.fi/URN:ISBN:978-952-60-4846-8>



## Preface

The work presented in this thesis has been carried out at Department of Micro- and Nanosciences at Aalto University School of Electrical Engineering, formerly Helsinki University of Technology, during 2008-2012.

I would like to express my gratitude and deepest appreciation to Professor Markku Sopanen for supervising this thesis. I would also like to thank Professor Harri Lipsanen for providing me with the opportunity to conduct this research at Department of Micro- and Nanosciences.

I am personally grateful to Dr. Sami Suihkonen, my thesis instructor, for his continuous support and input during the past 5 years. His amazing ability of formulating logical conclusions to difficult problems was always a big relief. I would also like to thank the THY folks including Dr. Pekka Törmä, Mr. Olli Svensk and Mr. Sakari Sintonen for their active participation in this research and many fruitful discussions. During this research I also got a chance to work with many other talented people and I would specially like to mention Dr. Marco Mattila. He has been of great help at numerous occasions. I would also like to thank Dr. Maxim Odnoblyudov, Dr. Vladislav Bougrov and Dr. Alexei Romanov from Opto-GaN Group for support and collaboration during the previous years. I am also indebted to our research partners from Ioffe Physico-Technical Institute Russia for offering their expertise in transmission electron microscopic investigations. The Finnish Funding Agency for Technology and Innovation (TEKES) and Multidisciplinary Institute of Digitization and Energy (MIDE) are acknowledged for the financial support of this research work.

I would like to express a heartfelt appreciation for my parents, sister and brother. They have been a big source of motivation throughout my doctoral studies. And finally, how can I forget Sana, my wife and teetu beetu (the thesis baby) for their love, patience and support, especially during the last year.

Landshut, 15.05.2012

Muhammad Ali



# Contents

<b>Preface</b>	<b>v</b>
<b>Contents</b>	<b>vii</b>
<b>List of Publications</b>	<b>ix</b>
<b>Author's Contribution</b>	<b>xi</b>
<b>List of abbreviations</b>	<b>xii</b>
<b>1. Introduction</b>	<b>1</b>
<b>2. Properties of III-nitride semiconductors</b>	<b>5</b>
2.1 Crystal structure . . . . .	5
2.2 Band structure . . . . .	6
2.3 Polarization in III-nitrides . . . . .	9
2.4 Quantum wells . . . . .	10
<b>3. Growth of nitride semiconductors</b>	<b>13</b>
3.1 Substrates . . . . .	13
3.2 Basics of MOVPE . . . . .	14
3.3 Thomas Swan MOVPE system . . . . .	16
3.4 MOVPE growth of GaN on c-plane sapphire . . . . .	18
3.5 Growth of III-N alloys . . . . .	20
<b>4. Experimental methods</b>	<b>23</b>
4.1 GaN and sapphire etching . . . . .	23
4.2 Electron microscopy . . . . .	25
4.3 X-ray diffractometry . . . . .	28
4.4 Luminescence spectroscopy . . . . .	30
<b>5. III-N light emitting diodes (LEDs)</b>	<b>33</b>

5.1 Overview . . . . . 33

5.2 History of GaN-based LEDs . . . . . 34

5.3 Epitaxial structure of blue and near UV LEDs . . . . . 35

5.4 Challenges for GaN based LEDs . . . . . 36

**6. Light extraction techniques and quaternary nitride structures 39**

6.1 Shape controlled voids in pendeo epitaxial GaN . . . . . 39

6.2 Maskless sapphire roughening . . . . . 49

6.3 Quaternary nitrides for near UV emission . . . . . 52

**7. GaN LEDs and micro-display for a contact lens 59**

**8. Summary 65**

**Bibliography 67**

**Publications 79**

# List of Publications

This thesis consists of an overview and of the following publications which are referred to in the text by their Roman numerals.

**I** M. Ali, A.E. Romanov, S. Suihkonen, O. Svensk, P.T. Törmä, M. Sopanen, H. Lipsanen, M.A. Odnoblyudov and V.E. Bougrov. Void shape control in GaN re-grown on hexagonally patterned mask-less GaN. *Journal of Crystal Growth*, 315, 188 (2011).

**II** M. Ali, A.E. Romanov, S. Suihkonen, O. Svensk, S. Sintonen, M. Sopanen, H. Lipsanen, V.N. Nevedomsky, N.A. Bert, M.A. Odnoblyudov and V.E. Bougrov. Analysis of threading dislocations in void shape controlled GaN re-grown on hexagonally patterned mask-less GaN. *Journal of Crystal Growth*, 344, 59 (2012).

**III** M. Ali, O. Svensk, L. Riuttanen, M. Kruse, S. Suihkonen, A.E. Romanov, P.T. Törmä, M. Sopanen, H. Lipsanen, M.A. Odnoblyudov and V.E. Bougrov. Enhancement of near-UV GaN LED light extraction efficiency by GaN/sapphire template patterning. *Semiconductor Science and Technology*, 27, 082002 (2012).

**IV** P.T. Törmä, O. Svensk, M. Ali, S. Suihkonen, M. Sopanen, M.A. Odnoblyudov and V.E. Bougrov. Maskless roughening of sapphire substrates for enhanced light extraction of nitride based blue LEDs. *Solid-State Electronics*, 53, 166 (2009).

**V** S. Suihkonen, O. Svensk, P.T. Törmä, M. Ali, M. Sopanen, H. Lipsanen,

M.A. Odnoblyudov and V.E. Bougrov. MOVPE growth and characterization of InAlGa<sub>N</sub> films and InGa<sub>N</sub>/InAlGa<sub>N</sub> MQW structures. *Journal of Crystal Growth*, 310, 1777 (2008).

**VI** M. Ali, S. Suihkonen, O. Svensk, P. T. Törmä, M. Sopanen, H. Lipsanen, M.A. Odnoblyudov and V.E. Bougrov. Study of composition control and capping of MOVPE grown InGa<sub>N</sub>/In<sub>*x*</sub>Al<sub>*y*</sub>Ga<sub>1-*x-y*</sub>N MQW Structures. *Physica Status Solidi (c)*, 5 , 3020 (2008).

**VII** A.R. Lingley, M. Ali, Y. Liao, R. Mirjalili, M. Klöner, M. Sopanen, S. Suihkonen, T. Shen, B.P. Otis, H. Lipsanen and B.A. Parviz. A single pixel wireless contact lens display. *Journal of Micromechanics and Microengineering*, 21, 125014 (2011).

# Author's Contribution

## **Publication I: “Void shape control in GaN re-grown on hexagonally patterned mask-less GaN”**

The author has written the manuscript, designed experiments, performed the major part of epitaxial growth of samples, sample processing, data collection and data analysis for publication I.

## **Publication II: “Analysis of threading dislocations in void shape controlled GaN re-grown on hexagonally patterned mask-less GaN”**

The author has written the manuscript, designed experiments, performed the major part of epitaxial growth of samples, sample processing and some parts of data analysis in publication II.

## **Publication III: “Enhancement of near-UV GaN LED light extraction efficiency by GaN/sapphire template patterning”**

The author has written the manuscript, designed experiments, performed the major part of epitaxial growth of samples, LED mesa etching, contact deposition and data analysis for publication III.

## **Publication IV: “Maskless roughening of sapphire substrates for enhanced light extraction of nitride based blue LEDs”**

The author has contributed to design of experiments and sample preparation for publications IV.

**Publication V: “MOVPE growth and characterization of InAlGaN films and InGaN/InAlGaN MQW structures”**

The author has contributed to the design of experiments, sample preparation and data analysis for publications V.

**Publication VI: “Study of composition control and capping of MOVPE grown InGaN/In<sub>x</sub>Al<sub>y</sub>Ga<sub>1-x-y</sub>N MQW Structures”**

The author has written the manuscript, designed experiments, performed the major part of epitaxial growth of samples, sample processing, data collection and analysis for publication VI.

**Publication VII: “A single pixel wireless contact lens display”**

The author has contributed to the writing of manuscript and designing experiments, performed epitaxial sample fabrication and part of sample processing for publication VII.

# List of abbreviations

AFM	atomic force microscopy
AlN	aluminium nitride
CBM	conduction band minimum
CCS	close coupled showerhead
EBL	electron blocking layer
EL	electroluminescence
ELOG	epitaxial lateral overgrowth
FWHM	full width at half maximum
GaN	gallium nitride
HVPE	hydride vapor phase epitaxy
I-V	current-voltage
ICP-RIE	inductively coupled plasma reactive ion etching
InN	indium nitride
IQE	internal quantum efficiency
IR	infra red
LED	light emitting diode
LEE	light extraction efficiency
LT	low temperature
MBE	molecular beam epitaxy
MOVPE	metal organic vapor phase epitaxy

MQW multi quantum well

PE pendeo epitaxy

PECVD plasma enhanced chemical vapor deposition

PL photoluminescence

PSS patterned sapphire substrates

QCSE quantum-confined Stark effect

QWs quantum wells

RT room temperature

SEM scanning electron microscopy

TDs threading dislocations

TEM transmission electron microscopy

TMA trimethylaluminium

TMGa trimehtylgallium

TMI trimethylindium

UV ultra violet

VBM valence band maximum

# 1. Introduction

The field of optoelectronics has undergone an unprecedented advancement during the last few decades. The impetus behind this progress has been the realization that optoelectronic devices will have far reaching benefits for human society in the 21<sup>st</sup> century. Silicon has long been and still is the conventional and most widely used semiconductor material. However, an inherent drawback of silicon as an optoelectronic material is its indirect energy band gap. The direct band gap of most of the III-V semiconductors gives them an obvious advantage over silicon and this has made III-V materials absolutely critical for modern day optoelectronic devices. Another advantage of these compound semiconductor materials is that the energy band gap can be tuned in a wide range when particular elements from group III and V of periodic table are combined. The tunable range of energy band gap covers the ultra-violet (UV), visible and infrared (IR) region of the electromagnetic spectrum.

Compound III-V semiconductors have shown remarkable potential in numerous applications ranging from ordinary transistor based electronics to optoelectronics. Light emitting diodes (LEDs) and laser diodes (LDs) based on III-V materials have matured into readily available commercial devices. LED based light sources have already started replacing conventional light bulbs and fluorescent lights. The superiority of LEDs over the other available options comes from the fact that they are highly energy efficient, have long lifetimes and affordable price. Furthermore, the possibility of accurately tuning the wavelength in a broad range of electromagnetic spectrum makes LEDs an attractive option for lighting applications.

The compound III-V semiconductors have traditionally been, divided into two main groups, *i.e.*, the conventional III-Vs and III-nitrides. The con-

ventional III-Vs that include phosphides, arsenides and antimonides are treated separately from nitrides due to a large difference in their crystal structure and growth conditions. Historically, the development of conventional III-Vs has remained far ahead of nitrides. This can be ascertained from the fact that first visible red LEDs based on arsenides were commercially rolled out in 1960s [1]. The conventional III-Vs have shown their dominance for devices operating in red and IR region of the electromagnetic spectrum. Theoretically the band gap of III-nitrides (InN, GaN and AlN) can be tuned all the way from the UV to IR region of the electromagnetic spectrum. However, the progress in the development of nitride based optoelectronic devices has the disadvantage that the growth process for good quality nitrides was invented as late as in the 1990s. Also the lack of availability of native substrates and difficulties in p-type doping slowed down the development of first commercial nitride based LEDs. It was in mid 1990s when this milestone was achieved. As of today, high brightness blue LEDs are currently the primary and most widely used application of GaN based materials. Phosphor coated blue LEDs are being used to generate white light for indoor/outdoor lighting applications.

In addition to applications in general lighting, the LEDs are enabling novel technologies like miniaturized displays for augmented reality applications [2]. The idea of augmented reality enabled wearable computers certainly seems to be the next step that can revolutionize the way humans interact with their surroundings. The futuristic idea of accessing information via data super-imposed on one's field of vision is not science fiction anymore. Efforts towards making finished products in the form of head-mount or eyeglasses based wearable displays have turned out to be successful [3]. A bionic contact lens could be the next big thing, since it offers simpler and less cumbersome display option for augmented reality based applications.

This thesis discusses some key issues associated with the light output performance of GaN LEDs. Some new ideas to growth and efficiency enhancement of blue/near-UV light emitting structures are proposed. The thesis also discusses the successful demonstration of using blue LEDs for an augmented reality application. This thesis has been organized as follows: Chapter 2 gives an overview of fundamental properties of III-N materials. The important issues related to growth of GaN-based materials are discussed in Chapter 3. Chapter 4 presents some important processing and characterization techniques that were used during this research.

A short history of III-N LED related research and important technological developments along with the key challenges has been reviewed in Chapter 5. The main results of publications I-VI have been summarized in Chapter 6. The key details related to the proposed light extraction techniques in blue LEDs and growth of near-UV quantum well structures are presented in this chapter. Chapter 7 describes the use of GaN LEDs for an augmented reality application. Chapter 8 summarizes the important results of this thesis. The relevant publications of this work are attached at the end of this thesis.



## 2. Properties of III-nitride semiconductors

This chapter gives a basic overview of the crystalline structure and other important properties of group III-nitrides that are crucial in understanding the unique nature of these materials. The topics discussed in this chapter also provide an insight into some basic concepts which are of great importance for understanding the working principles of semiconductor quantum well (QW) based light emitting sources.

### 2.1 Crystal structure

The classification of solid materials is based on the internal atomic arrangement. Materials having highly ordered and periodic atomic arrangement are classified as crystalline whereas materials with random atomic arrangement are grouped together as amorphous materials. The typical characteristic properties of semiconductors are associated to their periodic atomic arrangement which is also known as the lattice structure. III-N semiconducting materials can crystallize into hexagonal wurtzite, cubic zinc blende or rocksalt crystal structure [4]. Owing to its thermodynamic stability under ambient conditions, the wurtzite structure has been studied extensively and is used in most of the optoelectronic applications. The samples fabricated and analysed in this study were grown under conditions favoring wurtzite type crystal structure. Thus, the remainder of the thesis will focus exclusively on this type of crystal structure.

The wurtzite structure has a hexagonal non-primitive unit cell and thus two lattice constants. As an example, a hexagonal unit cell for GaN is shown in Fig. 2.1. It contains two interpenetrating hexagonal close packed (hcp) sub-lattices, each consisting of 6 group III or nitrogen atoms only. The lattice atoms are bonded to the nearest neighbor in tetrahedral pattern and the unit cell is described by the lattice parameters  $a$ ,  $c$  and  $a$

dimensionless parameter  $u$ .

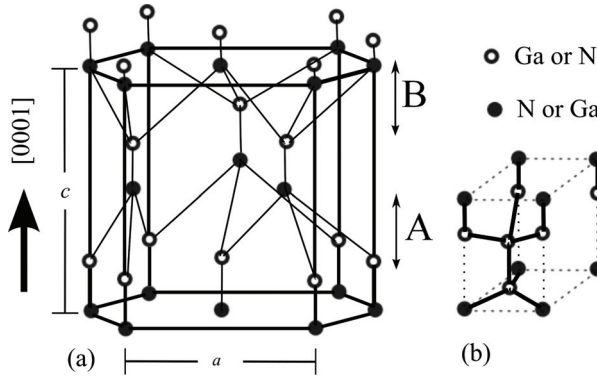


**Figure 2.1.** (a) Hexagonal wurtzite crystal structure of GaN and (b) unit cell of wurtzite GaN.

The lattice parameter  $a$  defines the edge length of the hexagonal basal plane, and the lattice parameter  $c$  describes the spacing in between two identical hexagonal lattice planes. The dimensionless parameter  $u$  characterizes the bond length along the  $c$ -direction. For an ideal hexagonal lattice,  $u=3/8$  and deviation from this value provides information about the distortion of the unit cell. The hexagonal bi-layers in wurtzite GaN follow an  $.....ABABAB.....$  sequence as marked in Fig. 2.1. Lattice parameters  $a$ ,  $c$  and dimensionless parameter  $u$  for binary nitrides are given in Table 2.1.

**Table 2.1.** Lattice parameters  $a$ ,  $c$  and  $u$  for binary nitrides [5].

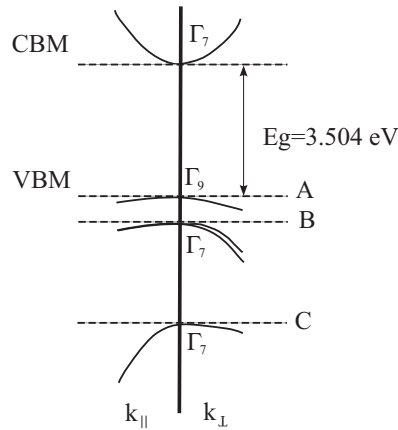
Lattice parameter	AlN	GaN	InN
$a$ ( $\text{\AA}$ )	3.111	3.189	3.534
$c$ ( $\text{\AA}$ )	4.978	5.185	5.718
$u$	0.379	0.377	0.382

## 2.2 Band structure

The periodic arrangement of atoms in a crystal merges the energy levels of various electrons present in different orbits. These closely spaced energy

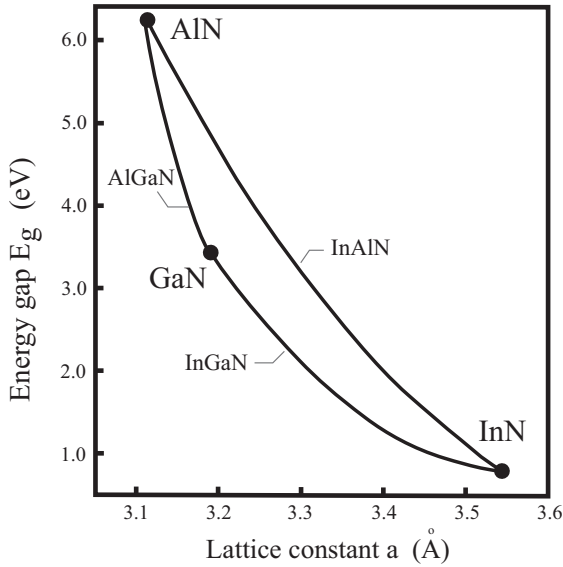
levels are called energy bands, which allow the movement of electrons in the crystal. The merging of energy levels associated with the outer-shell electrons leads to the formation of conduction band (CB) whereas merging of the energy levels associated with the inner-shell electrons forms valence band (VB). The energy gap that separates the CB and VB is called the energy band gap ( $E_g$ ). The classification of materials into conductors, insulators and semiconductors is associated to the size of energy band gap which could be nonexistent, large or small (relative to 2-5 eV), respectively. In semiconductors, this band gap could either be direct or indirect. In the case of direct band gap semiconductors, the valence band maximum (VBM) and conduction band minimum (CBM) have the same value of wave vector  $\vec{k}$  which is not the case in indirect band gap semiconductors. The probability of an optical transition from CBM to VBM is much lower with the assistance of a phonon which is required in indirect band gap semiconductors. This makes the direct band gap semiconductors much more suitable for light emitting devices [6]. III-N semiconductors belong to this class of semiconductor which have direct band gap.

Fig. 2.2 shows the calculated band structure of hexagonal wurtzite GaN near the fundamental gap  $\vec{k}=0$  in the  $\tilde{k}$ -space. The band gap value ( $E_g$ ) is calculated at a temperature of 40 K. As can be seen, the CBM and VBM have the same  $\tilde{k}$ -value, and the VB is split in three different sub-bands (A, B and C) by crystal field and spin orbit coupling. The III-nitride material system is extremely versatile because the direct band gap values span from 0.64 eV (IR region) of InN to 6.14 eV (deep-UV) for AlN [7].



**Figure 2.2.** Calculated band structure near the  $\Gamma$  point of hexagonal wurtzite GaN. The top of the valence band is split into three different bands by the crystal field (band C) and by the spin-orbit coupling (band B). Modified from [8].

Fig. 2.3 shows band gap energy versus the lattice constant  $a$  for III-nitride materials. The possibility of alloying III-nitrides to form ternary (AlGaN, InGaN, InAlN) and quaternary ( $\text{In}_x\text{Al}_y\text{Ga}_{1-x-y}\text{N}$ ) alloys makes them particularly attractive for many optoelectronic applications.



**Figure 2.3.** Band gap energy versus lattice constant  $a$  in the III-nitride materials system.

The compositional dependence of the band gap for ternary alloys can be calculated from [9, 10]

$$E_g(A_xB_{1-x}C) = xE_g(AC) + (1-x)E_g(BC) - x(1-x)C_{ABC}, \quad (2.1)$$

where the first two terms on the right-hand side of the equation give a linear interpolation of the band gap energy and the third term represents the deviation from this linear value for the ternary alloy  $A_xB_{1-x}C$ . The constant  $C_{ABC}$  is called the bowing parameter. Similarly, compositional dependence of the band gap for quaternary alloys can be calculated from a more complicated empirical expression given by [11, 12]

$$E_g(x, y) = xE_g(\text{InN}) + yE_g(\text{AlN}) + (1-x-y)E_g(\text{GaN}) - b_{\text{Al}}y(1-y) - b_{\text{In}}x(1-x), \quad (2.2)$$

where the fourth term represents the bowing contribution related to Al and the last term represents the bowing contribution due to In. The parameters  $x$  and  $y$  represent the molar fractions of binaries InN and AlN, respectively.

### 2.3 Polarization in III-nitrides

As it has been already discussed in section 2.1, the atoms in hexagonal wurtzite structure of nitrides are located in an alternating sequence of monolayers comprising of group III species and N in the  $\pm c$  direction. Such an arrangement of atoms leads to a lack of central inversion symmetry. This means that the direction of the atomic bonds are different along the  $[000\bar{1}]$  and  $[0001]$  directions. Hence, there exists a polarity in the films along the  $c$ -direction. Fig. 2.4 shows the two different polar orientations of GaN. When the bonds along the  $c$ -direction are from Ga to N, the film is termed as Ga-polar. In this case the direction of bonds from Ga to N along the  $c$ -direction marks the  $[0001]$  direction. Similarly, when the bonds along the  $c$ -direction are from N to Ga, the polarity is termed as N-polar. In such a scenario the direction of bonds from N to Ga along the  $c$ -direction marks the  $[000\bar{1}]$ .

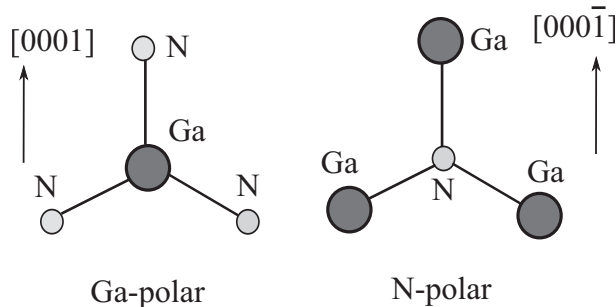


**Figure 2.4.** Ball and stick configuration of atoms in the Ga- and N-polar arrangement in wurtzite GaN.

It has been experimentally shown that the type of growth method influences the polarity of GaN grown on (0001) sapphire substrate. The films grown with metalorganic vapor phase epitaxy (MOVPE) turn out to be Ga-polar while the films grown by molecular beam epitaxy (MBE) are commonly N-polar [12, 13, 14]. All the samples studied in this thesis were grown by MOVPE and were Ga-polar.

In the absence of any external electric field the total polarization is a sum of spontaneous polarization ( $P_{sp}$ ) and piezoelectric polarization ( $P_{pz}$ ). Spontaneous polarization in wurtzite nitrides originates due to the polar nature of these materials. On the other hand, piezoelectric polarization stems out from the fact that hetero-epitaxial layers are inherently strained.  $P_{pz}$  can be expressed as the sum two independent piezoelectric

coefficients  $e_{31}$  and  $e_{33}$  [15]

$$\delta p = e_{33} \frac{c - c_0}{c_0} + 2e_{31} \frac{a - a_0}{a_0}, \quad (2.3)$$

where  $c_0$  and  $a_0$  are the equilibrium values of out-of-plane and in-plane lattice parameters. Piezoelectric coefficients in III-N materials are found to be ten times larger than in conventional III-V and II-VI semiconductor compounds [15, 16]. The presence of spontaneous and piezoelectric polarization causes an internal electric field in the material [17, 18]. The built in electric field in III-N wurtzite materials is discussed in more detail later.

## 2.4 Quantum wells

A QW is a structure consisting of a semiconductor having a smaller band gap energy sandwiched between materials with larger band gap energies. The carrier (electrons and/or holes) see a lower potential in the well layer and become confined into this layer. The energy levels are discrete, perpendicular to the layer and continuous in the two dimensions along the layer. The phenomenon of quantum confinement comes into action when the thickness of the QW becomes comparable to the *de Broglie* wavelength of the carriers. The spatial confinement of carrier charges and the corresponding modification of the density of states results in high radiative efficiencies, low laser threshold currents and reduced surface recombination effects in QW structures as compared to bulk materials. QWs are particularly advantageous, since they give the flexibility of engineering the energy levels by combination of different band gap semiconductors. It is because of this and high radiative efficiencies that QWs are considered crucial for modern day LEDs and LDs.

As it has been discussed in the previous section, piezoelectric polarization is induced as a result of strain in a layer. The nitride layers grown on foreign substrates are under bi-axial strain and, thus, have high values of built in electric field. Usually the value of this field is of the order of  $10^6$  V/cm [19]. The total built-in electric field is equal to the sum of spontaneous ( $E_{sp}$ ) and piezoelectric fields ( $E_{pz}$ ). Depending on the directions of these fields, piezoelectric field can add up to strengthen or weaken the spontaneous field in the layer. For the case of InGaN/GaN QWs, the InGaN layers are under compressive stress. Hence, the directions of  $E_{sp}$  and  $E_{pz}$  are opposite to each other. The value of total built in field for typical

$\text{In}_{0.22}\text{Ga}_{0.78}\text{N}/\text{GaN}$  QWs can be as high as 3.1 MV/cm [20]. Nevertheless, the presence of this large electric field in such a heterostructure leads to significant band bending. The band bending results in the conduction band minimum to be energetically close to the valence band maximum, thus effectively reducing the band gap. This reduction redshifts the wavelength and is known as quantum confined Stark effect (QCSE). The band bending increases the spatial separation of electron and hole wavefunctions by pushing them towards opposite sides of the QW. This separation means that the overlap between the two wavefunctions is reduced compared to flat-band situation that is the case in zero-field scenario (Fig. 2.5). A decrease in the overlap reduces the probability of effective radiative recombination. This is particularly true for thick QWs, *e.g.*, thicker than 100 Å. For this reason the QW thicknesses of 20 – 30 Å are typically used to minimize such electron-hole separation effects [21]. InGaN/GaN QWs are known to undergo a blue shift in their wavelength at high carrier densities. Coulomb screening of the QCSE and band filling of localized states by excitons are two well documented reasons for the blueshift behavior at high carrier densities [22, 23]. Hence, the decrease in the overlap of electron-hole wavefunction can be recovered. The doping of barriers with Si has also been reported to increase the electron-hole wavefunction overlap [24].

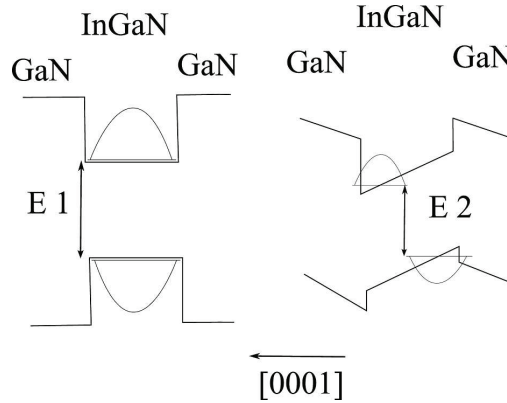


**Figure 2.5.** Schematic illustration of un-strained ( $E_1$ ) and strained ( $E_2$ ) InGaN/GaN QW, where  $E_2 < E_1$  due to QCSE.

The effect of internal electric field can be reduced by growing the material along the non-polar or semi-polar crystal directions. In practice this is done by using non-polar or semi-polar substrates. In non-polar case ( $a$ -plane), the piezoelectric field is perpendicular to the growth direction. Such direction of internal electric field does not influence the position of

electron-hole wavefunction in the active device layers [25]. All the samples in this work were grown on c-plane surface, and thus have internal electric field along the growth direction.

### 3. Growth of nitride semiconductors

Growth of III-nitride materials is a very interesting yet a challenging task. Starting from the issue of substrates and then moving onto the explanation of epitaxial growth of different nitride layers, this chapter gives a general overview for the some of the key topics that are associated with this research work.

#### 3.1 Substrates

The most desirable form of semiconductor epitaxy is when it is performed on a native substrate. The biggest motivation to follow this route is the desire to avoid interface effects and decrease the probability of defect formation. Unfortunately, the III-nitride material system still lacks the wide availability of cost effective native substrates compared to other III-V materials. This shortcoming is due to the presence of many technological challenges that hinder the growth of nitride materials in bulk form [26]. Hence, growth of III-N materials is mostly based on heteroepitaxial techniques. In heteroepitaxy, the lattice mismatch between the substrate and the growing film is mainly responsible for the formation of stacking faults and threading dislocations (TDs). Furthermore, a difference in the thermal expansion coefficient of the two may lead to crack generation in the grown film. The group III-nitrides have been grown on a wide variety of substrates including  $\text{Al}_2\text{O}_3$  (c-, a-, m- and r-planes), SiC, ZnO, Si, ZnO,  $\text{LiGaO}_2$  and  $\text{ScAlMgO}_4$  [27].

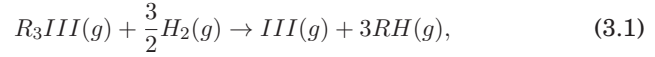
SiC and  $\text{Al}_2\text{O}_3$  (sapphire) are by far the most commonly used substrates for GaN epitaxy. SiC has very good thermal conductivity and much smaller lattice mismatch with GaN compared to sapphire. However, SiC has a smaller in-plane thermal expansion coefficient with respect to GaN. This leads to the generation of tensile stress in the GaN epi-layer as the films

are cooled down after growth. Furthermore, SiC substrates are comparatively expensive. On the other hand, sapphire substrates offer good thermal stability at high temperature that is usually required for the growth of GaN epi-layers. It is transparent in nature, has relatively low cost and is available in large diameter sizes. The lattice mismatch between wurtzite GaN and c-plane sapphire substrates is huge (49%) [27]. The heteroepitaxial growth across the GaN and sapphire interface is dictated by the Al–O bonding on the sapphire surface, which results in a 30° in-plane rotation of the nitride lattice with respect to the sapphire substrate. The commonly mentioned lattice mismatch of ~16% is a result of this rotational alignment of the GaN hexagonal base [28, 29]. This lattice mismatch is still quite high compared to many other substrates. Apart from this, the in-plane thermal expansion coefficient of sapphire substrates is higher than that of GaN. This results in compressively strained GaN films on cooling down to room temperature [30].

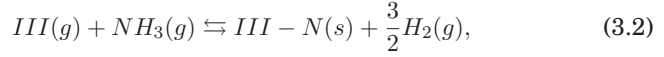
### 3.2 Basics of MOVPE

A wide variety of growth techniques including liquid phase epitaxy (LPE), hydride vapor-phase epitaxy (HVPE), chemical beam epitaxy (CBE), MBE and MOVPE have been employed to grow III-nitrides. Owing to its flexibility in growing a variety of high purity materials with accurate composition, thickness and doping along with large scale growth at reasonable growth rates, MOVPE is by far the most popular method employed for growth of nitrides. The popularity of the MOVPE technique has seen a significant increase since the development and rapid commercialization of blue, green and yellow LEDs and blue lasers [31, 32, 33].

MOVPE is a thin-film growth process involving the vapor transport of precursor molecules towards a heated substrate. After reaching the hot zone, the gaseous species are “cracked” which leads to a series of chemical reactions between the cracked reactive components and the substrate surface. In the most basic form we can consider four incoming vapor species, namely, metalorganic containing group three element ( $R_3III$ ), ammonia ( $NH_3$ ), hydrogen ( $H_2$ ) and inert gas such as nitrogen ( $N_2$ ). If we assume that the group-III and –V precursors are mixed only above the substrate then we can neglect the chance of pre-reactions. The irreversible pyrolysis reaction occurring at the vapor-solid interface can be written as [34]



where (g) represents the respective constituents in the gas phase. The chemical reaction occurring at the substrate surface for binary nitrides can be expressed as



where (g) and (s) represent the gas and solid phases, respectively. The reaction described in Eqn. 3.2 can proceed in forward direction representing the deposition process and in reverse direction for an etching process. The amount of hydrogen on the right hand side of Eqn. 3.2 strongly governs the reversibility of this equation at high temperatures.

Vapor phase epitaxy (VPE) is a complex process. Different surface processes such as adsorption, desorption and surface migration contribute towards the film growth. It is generally agreed that the growth rate as a function of temperature can broadly be divided into three different regimes [35]. Fig. 3.1 shows the growth rate as a function of temperature and the associated growth regimes.

The low temperature growth regime in Fig. 3.1 is governed by the reaction rates of the reactable species at the surface, hence referred to as a kinetically limited domain. The effective temperature range of kinetically limited regime is based on the pyrolysis efficiencies for a set of incoming compounds. For example, in the case of Ga- and In-alkyl compounds kinetically limited regime occupies a very narrow temperature range since the pyrolysis efficiencies of these alkyls rise very steeply with rising temperatures [35]. Since  $NH_3$  is utilized as an active source of nitrogen in the MOVPE process, its decomposition efficiency is also an important factor to consider. Under equilibrium conditions,  $NH_3$  is expected to decompose into  $N_2$  and  $H_2$  at temperatures higher than 300 °C, however the cracking efficiency is too low. It is known that in the absence of catalyst the decomposition rate of  $NH_3$  is slow. Furthermore, the decomposition also shows some dependence to the growth conditions and equipment used [36, 37].

In the intermediate temperature range the chemical reaction rates are much higher. In such a scenario, the mass transport of gaseous species to and away from the surface has the most influential role in the film growth. Since the gas phase diffusion of alkyls is only a weak function of temperature, the growth rate remains nearly unaffected by the temperature variations [35]. This region typically has a range of few hundred

degrees Celsius. In the third regime, the VPE process is thermodynamically limited. As a result of increasing temperature the chances of gas phase reactions are increased along with increased desorption rates and depletion of reactants on the reactor walls. The gas inlet design and the reactor geometry need a thorough evaluation to minimize the effects of thermodynamically limited regime.

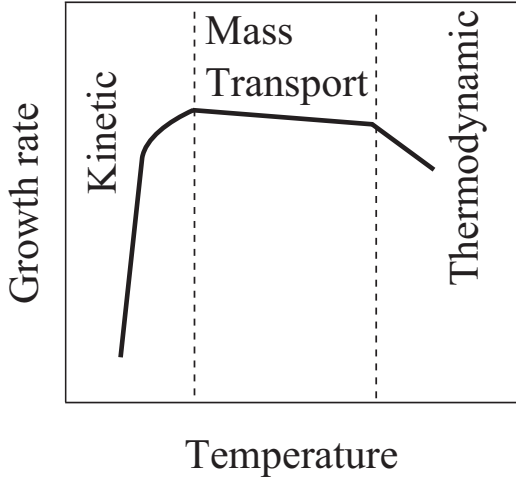


**Figure 3.1.** Temperature dependence of growth rate in VPE process for kinetically, mass transport and thermodynamically limited regimes.

### 3.3 Thomas Swan MOVPE system

A close-coupled showerhead (CCS) MOVPE system made by Thomas Swan Scientific Equipment was used for the epitaxial growth of III-N layers in this thesis. The gas flow diagram for the MOVPE system at Micronova is shown in Fig. 3.2. In this system gaseous  $\text{NH}_3$  and disilane ( $\text{Si}_2\text{H}_6$ ) were used as nitrogen and silicon sources, respectively. The disilane was diluted in hydrogen in 100 parts per million (ppm) concentration. The liquid metalorganic precursors are located inside small cylindrical shaped metal containers known as bubblers. The bubblers are kept in temperature controlled baths, since vapor pressures of precursors are extremely sensitive to temperature. In this system trimethylgallium (TMGa), trimethylaluminium (TMAI), trimethylindium (TMIn) and bis(cyclopentadienyl) magnesium ( $\text{Cp}_2\text{Mg}$ ) are used as gallium, aluminium, indium and magnesium sources, respectively.  $\text{H}_2$  and  $\text{N}_2$  are used as carrier gases for transporting the metal-organics to the reactor. Mass flow controllers are used to

regulate the gas flows into the reactor. A fast and efficient switching of precursors allows the growth of low dimensional structures such as QWs with sharp interfaces. Separate carrier lines are used to transport the group III and V species in order to avoid any pre-reactions.

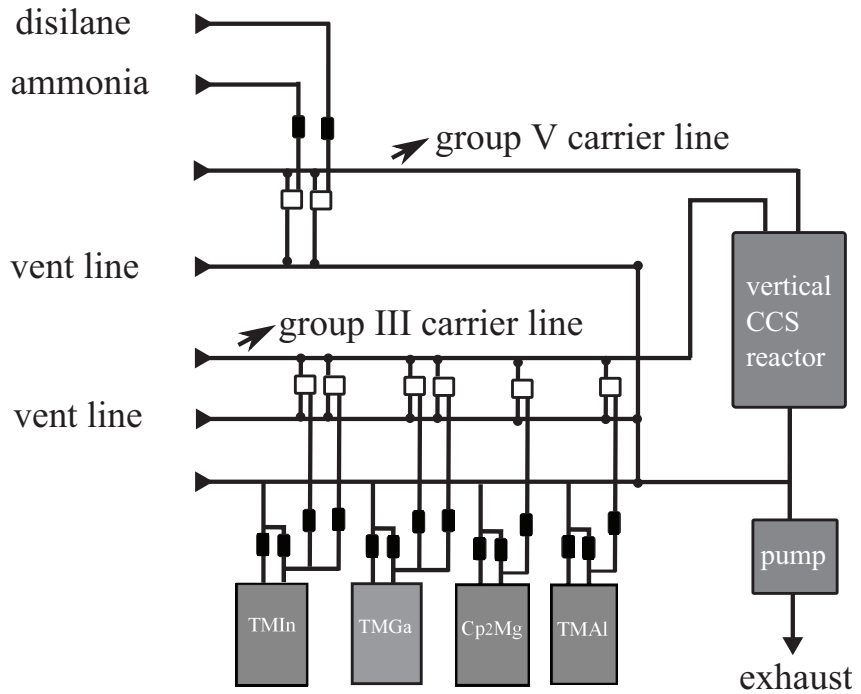


**Figure 3.2.** A simplified gas flow diagram of MOVPE system used in this work.

Fig. 3.3 shows a cross-sectional view of the MOVPE reactor used in this work. The reactor design is based on showerhead type gas inputs which ensures a uniform gas flow over the wafers. This showerhead is connected to the precursor lines. The wafers are placed on a SiC coated graphite susceptor, which is heated from underneath with a help of tungsten heater coils. The horizontal and vertical gas flow ratios are controlled by rotating the susceptor during epitaxial growth. The temperature of this reactor system can be effectively controlled up to 1200 °C. All the temperature values mentioned in this thesis are thermocouple readings measured just below the susceptor. The reactor was calibrated to  $\pm 3$  °C variation across the wafer. The pressure inside the reactor has a controllable range of 50 – 900 Torr. An in-situ monitoring system is also installed on top of the reactor. The reflected intensity of normally incident laser light beam with a wavelength of 635 nm is measured to monitor growth and the thickness of the epitaxial layers. The in-situ reflectance is employed to gain critical information during the nucleation and coalescence of epi-layers.

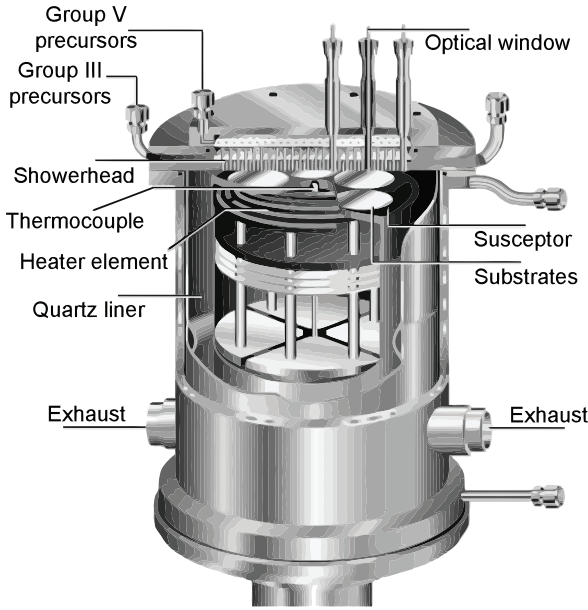


**Figure 3.3.** Cutaway view of the Thomas Swan MOVPE reactor [38].

### 3.4 MOVPE growth of GaN on c-plane sapphire

Since the GaN bulk layers (*i.e.*, GaN templates) are an integral part of all the heterostructures fabricated in this thesis, it is considered necessary to give an overview of the MOVPE growth process for these layers.

One of the earliest reports of single crystalline GaN date back to 1969, when Maruska *et al.* reported GaN specimens of reasonable electrical and optical quality [39]. Since then efforts were made to improve the quality of GaN. It was in 1980's when Amano *et al.* reportedly used a 50 – 100 nm thick AlN nucleation layer (NL) grown at low temperature (LT) followed by high temperature growth of GaN layer [40]. This type of growth process enhanced the surface morphology and the electrical and optical properties of GaN grown on sapphire. Later on Nakamura reported growth of high quality GaN using a GaN nucleation layer with a similar two-step approach [41]. Fig. 3.4 shows the process flow of the two-step method that is commonly employed for growth of GaN layers on sapphire.

A flow of hydrogen carrier gas is present throughout the process. The sapphire substrate is heated to temperatures in excess of 1050 °C for the removal of impurities from the surface. Temperature is then decreased

and  $\text{NH}_3$  is introduced into the reaction chamber at around  $800^\circ\text{C}$ . This initiates the nitridation of the sapphire surface and, thus, forms a thin  $\text{AlN}$  layer on the substrate. The duration of  $\text{NH}_3$  flow is considered to be an important factor for this step [42]. With  $\text{NH}_3$  flow still on, the temperature is reduced to about  $530^\circ\text{C}$ . At this point the  $\text{TMGa}$  flow is switched on. Under these conditions the  $\text{GaN}$  NL is formed and growth is continued until a nominal layer thickness of  $40 - 100\text{ nm}$  is achieved. At this point the LT  $\text{GaN}$  is comprised of both the cubic and the hexagonal crystal structures [43, 44].

After growth of the LT nucleation layer,  $\text{TMGa}$  flow is switched off and temperature is ramped up to approximately  $1000^\circ\text{C}$  for the  $\text{GaN}$  growth. The ramping of temperature starts the recrystallization of the NL. A decomposition of disordered material along with its redistribution takes place giving rise to formation of  $\text{GaN}$  islands of hexagonal structure on the surface. At the start of high temperature growth the  $\text{GaN}$  islands grow both laterally and vertically (3D growth mode). As the growth continues, the islands grow bigger and finally they start merging with each other to form a smooth coalesced layer of  $\text{GaN}$ .

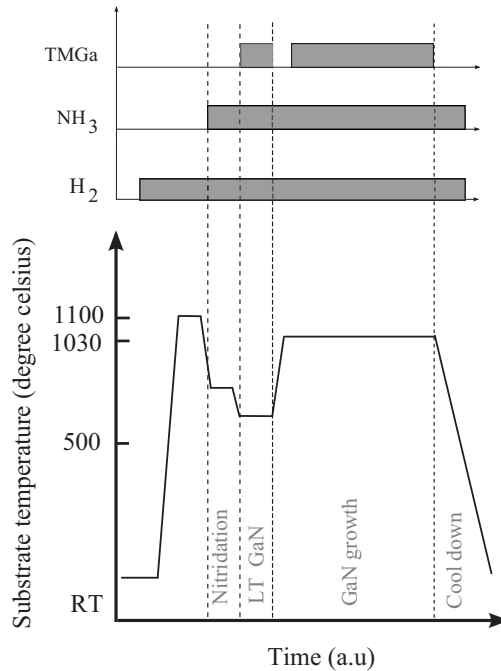


**Figure 3.4.** Time line of precursor flows with respect to temperature profile for the two-step growth of  $\text{GaN}$ .

### 3.5 Growth of III-N alloys

The possibility of alloying GaN with Al, In or a combination of both makes it a diverse material system. The ternary GaN alloys, *i.e.*,  $\text{In}_x\text{Ga}_{1-x}\text{N}$  and  $\text{Al}_y\text{Ga}_{1-y}\text{N}$  have been extensively studied in the last twenty years. Growth of ternary nitride alloys can be accomplished by mixing the vapors of different alloy constituents in an appropriate vapor phase ratio to achieve a desired composition.  $\text{In}_x\text{Ga}_{1-x}\text{N}$  layers are at the heart of the modern day LEDs and LDs operating in the sub-green to near UV wavelengths. On the other hand,  $\text{Al}_x\text{Ga}_{1-x}\text{N}$  layers have found their usage not only in UV and deep UV emitting structures but also as carrier blocking layers [45, 46, 47].

The band gap of ternary  $\text{In}_x\text{Ga}_{1-x}\text{N}$  varies from 3.4 to 0.64 eV as the In content is varied from 0 to 100 % [7, 48]. Bedair *et al.* have modeled the growth of  $\text{In}_x\text{Ga}_{1-x}\text{N}$  on the basis of competitive processes that occur during growth [49]. According to this model three reaction pathways can occur. Indium can either be incorporated in the solid ternary alloy, can be incorporated as metal droplets or desorbed from the growth surface. The occurrence of any specific reaction pathway is dependent on the growth conditions inside the reaction chamber. Out of various growth parameters the desorption of In shows an exponential dependence on growth temperature. This strong temperature dependence can be associated to the weaker InN bond strength which is 1.93 eV as compared to 2.2 eV for GaN and 2.88 eV for AlN [50, 51]. Hence, MOVPE growth of  $\text{In}_x\text{Ga}_{1-x}\text{N}$  layers is usually performed in a temperature range of 700 – 800 °C [42]. Higher concentration of In in the ternary films (> 20%) is particularly challenging due to the large lattice mismatch between InN and GaN, which is approximately 10 %. The type of carrier gas also plays a key role in In incorporation. It has been shown that the In content in the  $\text{In}_x\text{Ga}_{1-x}\text{N}$  layers decreases as partial pressure of  $\text{H}_2$  gas is increased during growth [52, 53].  $\text{N}_2$  was used as a carrier gas for the growth of  $\text{In}_x\text{Ga}_{1-x}\text{N}$  layers this work. The general trends of the In content of epitaxial  $\text{In}_x\text{Ga}_{1-x}\text{N}$  film growth in dependence of various MOVPE parameters is shown in table 3.1.

MOVPE growth of  $\text{Al}_y\text{Ga}_{1-y}\text{N}$  epitaxial layers on GaN has a different set of challenges when compared to  $\text{In}_x\text{Ga}_{1-x}\text{N}$  growth. The differences in the lattice mismatch, ionic radii, chemical reactivity with nitrogen and higher thermal stability requires a different set of growth conditions [52].

There have been several reports on the growth of  $\text{Al}_y\text{Ga}_{1-y}\text{N}$  layers at various temperatures in the range of  $800 - 1150^\circ\text{C}$  [54]. Growth of high quality crack and defect free  $\text{Al}_y\text{Ga}_{1-y}\text{N}$  layers with high Al content is still a challenging task. Another prominent issue which complicates the growth of  $\text{Al}_y\text{Ga}_{1-y}\text{N}$  is the occurrence of gas phase pre-reactions which decrease the incorporation efficiency of Al atoms [55, 56].

**Table 3.1.** Trends for In content in InGaN layers in dependence of various MOVPE growth parameters ( $\uparrow$ : increasing ,  $\downarrow$  : decreasing , O: weak influence) [52]

MOVPE parameter	In content	
Substrate temperature	$\uparrow$	$\downarrow$
Growth rate	$\uparrow$	$\uparrow$
Input In/(In+Ga) ratio	$\uparrow$	$\uparrow$
Hydrogen partial pressure	$\uparrow$	$\downarrow$
$\text{NH}_3$ partial pressure	$\uparrow$	O
Total pressure	$\uparrow$	O



## 4. Experimental methods

This chapter presents an overview of various experimental methods that were used for fabrication and characterization processes in this thesis.

### 4.1 GaN and sapphire etching

The group III nitrides are known for their high bond strength and chemical inertness which is reflected in their resistance to wet etching [57, 58]. For this reason a variety of process routes have been investigated by researchers for the etching of these materials. In broader terms, the etching methods commonly used for III-N materials fall into two categories, *i.e.*, wet etching and dry/plasma etching. The quest for achieving better control over isotropy with high etch rates has lead to extensive development of plasma etching techniques for nitrides. A significant number of investigations based on reactive ion etching (RIE) and inductively coupled plasma (ICP)-RIE have been carried to etch III-N materials [57]. Use of high density and low pressure plasma systems have shown excellent results for the patterning of group-III nitrides. The high plasma flux enhances the bond breaking efficiency in the nitrides and desorption of the etch products is effectively carried out in such systems [59]. ICP-RIE has been used as the dry etching method in this work.

For ICP-RIE of GaN,  $\text{Cl}_2$ - based gas chemistry has been used extensively [58]. Hydrogen based ICP-RIE etching process has also been reported. It is not commonly used, since the diffusion of hydrogen into GaN can potentially deactivate the dopants in GaN [60]. The plasma etching involves two general mechanisms: (a) chemical-based mechanism where reactive species formed in the plasma interact with the substrate and (b) a physical mechanism where energetic ions formed in the plasma sputter the sample surface. Etch processes dominated by chemical mechanisms tend

to be isotropic. Alternatively, physically dominated etch mechanisms initiate sputter desorption of substrate and/or etch products formed on the surface by high energy ions. An ICP-RIE system produces a high density discharge at low pressure which generates an efficient etching environment. Independent biasing of the sample with RF power provides control over the energy at which ions bombard the sample [61].

The ICP-RIE equipment utilized in this thesis was Oxford Plasmalab 100. A schematic diagram of the system is shown in Fig. 4.1. Both fluorine and chlorine based etch chemistries are available in the ICP-RIE system located at Micronova. The ICP source power can be adjusted to 2 kW while a maximum 300 W of capacitively coupled plasma (CCP) source power is available. The operating temperature can be varied from  $-150$  to  $400$  °C. The chamber pressure can be adjusted between 1 mT to 100 mT. Typical etch rates in the range of 400 – 500 nm/min can be achieved for GaN etching with  $\text{Cl}_2/\text{Ar}$  chemistry. The ICP system is connected to a single automated wafer transfer loadlock.

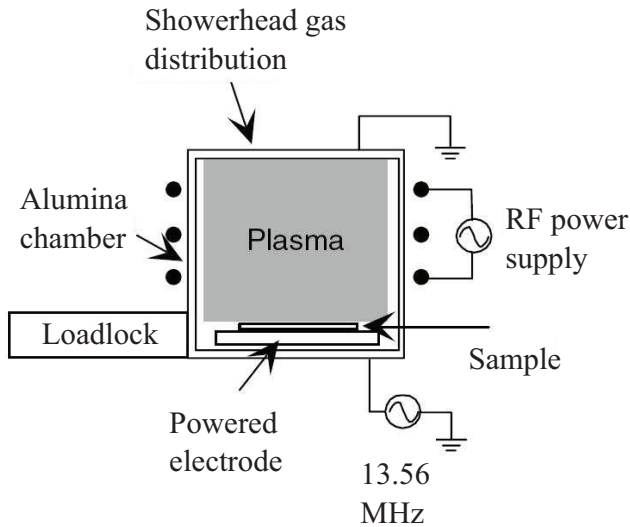


**Figure 4.1.** Schematic diagram of an ICP-RIE system.

There has been an increased interest towards the etching of sapphire since it has emerged as the most commonly used substrate for GaN LEDs. Etching sapphire is challenging due to the mechanically and chemically strong nature of sapphire. Good results have been reported by using either ICP-RIE or a wet etching process [62, 63]. In this thesis, a wet etching procedure was adopted for maskless etching the backside surface of the sapphire wafer. The standard commercial grade sulphuric acid

( $\text{H}_2\text{SO}_4$ ) or a mixture of  $\text{H}_2\text{SO}_4$  and phosphoric acid ( $\text{H}_3\text{PO}_4$ ) in the temperature range of 230 - 240 °C were used in our experiments <sup>1</sup> [ Publication IV]. A 1000 mL quartz chamber was used for acidic mixture and 2 inch wafer carrier was used to handle the wafers. The quartz chamber and wafer carrier were made of vacuum pressed quartz. For safety reasons, an additional cylindrical quartz casing was used to house the acid filled quartz chamber. A ceramic hotplate was used to heat up the quartz chamber. The ceramic hotplate temperature was accurately controllable to  $\pm 2$  °C . A quartz tube shielded thermocouple was used for an accurate temperature measurement inside the quartz chamber. The high temperatures used for the experiments created hot acid vapor during the process. A water cooled lid was used for the acid vapor condensation and the whole assembly was connected to a gas exhaust inside a fume hood. This setup ensured the safety of people working around the apparatus. Temperature, time, solubility of the etch products and acidity of the solution play a key role in determining the final etch rate of sapphire.

## 4.2 Electron microscopy

An electron microscope uses a controlled beam of electrons to produce an image or diffraction pattern. The electrons can be accelerated, focused and detected. The electrons have much shorter wavelength compared to photons in the visible spectrum. Thus, they can be used to illuminate a specimen and achieve higher resolution than with the optical microscope [64]. Depending on the total beam energy, nature and thickness of the specimen, a whole range of signals can be generated as a result of strong interaction between electron beam and the specimen. Fig. 4.2 shows an overview of various types of secondary signals that are generated as a result of this kind of interaction.

The generation of such a variety of signals gives the opportunity to detect them to provide qualitative or quantitative information about the specimen. The secondary and backscattered electrons are usually utilized in a scanning electron microscope (SEM). The elastically scattered electrons are utilized for transmission electron microscopy (TEM). In this thesis SEM and TEM techniques have been used to analyse the epitaxial lay-

---

<sup>1</sup> $\text{H}_2\text{SO}_4$  was 98 % pure with remaining balance of water.  $\text{H}_3\text{PO}_4$  was 85 % pure with remaining balance of water. Hot acids are extremely hazardous in nature. Appropriate working environment, suitable equipment and protective gear should be used when working with acids.

ers. Hence, the rest of this section focuses on providing an overview of necessary information required for a general understanding of these two microscopy techniques.

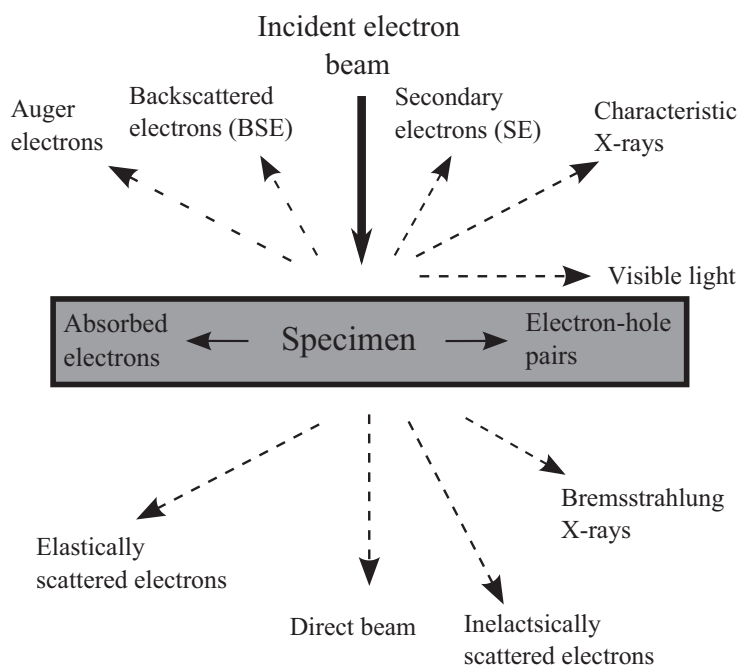


**Figure 4.2.** Different types of secondary signals generated as a result of interaction between the electron beam and the specimen.

SEM is perhaps one of the most popular tools among the scientists working in the field of micro- and nanotechnology. The reason behind its popularity can be associated to the fact that it offers high resolution, large depth of field and ease of sample preparation. A SEM is a mapping instrument in which a high energy electron beam is raster scanned over the specimen. A schematic illustration of the SEM imaging system is shown in Fig. 4.3. The electron source used in the SEM can be a tungsten filament or a Schottky emitter. An electron beam is accelerated in vacuum by a voltage typically in the range of 1-30 kV and focused on a narrow area having a spot size of few nanometers. Secondary electrons and backscattered electrons are commonly used for imaging samples. Secondary electrons are more useful for showing morphology and topography of the specimen. They are collected by attracting them towards an electrically biased detector. The exact beam spot position and the amplified signal from the detector are used together to generate the final image. Backscattered electrons are most valuable for illustration of contrast vari-

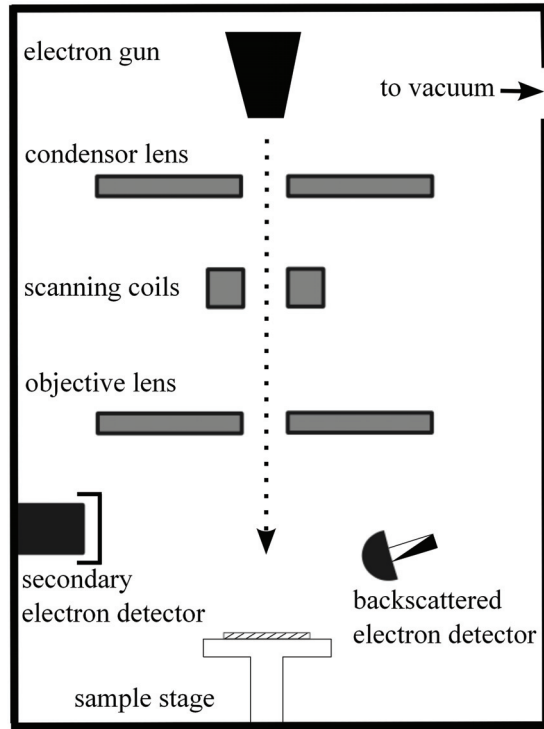


**Figure 4.3.** A simplified schematic block diagram of a SEM system.

ation in specimen regions with different atomic numbers. The proportion of backscattered electrons depends on the average atomic number of the sample and a difference in average atomic number is essential to distinguish different phases [65].

The sizes of the features studied in this thesis were in the range of few hundreds of nanometers to few micrometers. Hence, SEM was an ideal tool to analyse the layer structure of the samples. Top view and cross-sectional SEM images were taken for the evaluation of growth behavior and formation of voids in the patterned GaN templates [Publication I, II and III]. Similarly, tilted view SEM images were taken to analyse the roughening on sapphire substrates [Publication IV]. In this thesis Zeiss Supra 40 SEM was used for the structural characterization of the samples.

TEM is a very versatile tool and is conceptually analogous to the transmission optical microscope, in the arrangement of the specimen, the “light source” and the image plane. The difference lies in the fact that in TEM electrons are used instead of photons, and electrostatic and magnetic lenses

replace glass lenses. The detection is done with the aid of a fluorescent screen. Transmission electron diffraction pattern is formed from the electrons that pass through a very thin specimen. The diffracted electrons can be focused with the help of lenses to form an image. A TEM tool can be used to perform a wide range of experiments that involve conventional imaging (bright field (BF) and dark field (DF) TEM), phase-contrast imaging (high resolution TEM), selected area electron diffraction (SAED), convergent-beam electron diffraction (CBED), Z-contrast imaging, energy-dispersive x-ray spectroscopy (EDS) and electron energy-loss spectroscopy (EELS). In this thesis the specimens were prepared by mechanical thinning and ion milling process. The samples were analysed with conventional and phase-contrast imaging techniques. Multiple BF and DF TEM images were taken to study the behavior of TD propagation in GaN templates with embedded voids. TEM micrographs taken near the sidewall of the voids located at the GaN-sapphire interface were used to investigate bending phenomenon of TDs [Publication II]. All the sample preparation, TEM imaging and majority of TEM related analysis reported in this thesis was performed at Ioffe Physico-Technical Institute, Russia.

### 4.3 X-ray diffractometry

X-ray diffraction is a powerful non-destructive technique that is widely used to acquire information on the quality, structure, orientation and composition of crystalline materials. The interference pattern of elastically scattered x-rays can be understood on the basis of Laue condition. Alternatively, a much simpler explanation is given by Bragg's law according to which the constructive interference would only occur if the path difference between incident and diffracted beam is an integer multiple of wavelength.

A Philips X'pert high resolution X-ray diffractometer (HRXRD) was utilized in this work. The basic measurement setup is illustrated in Fig.4.4. A four crystal Ge monochromator is used to select the  $\text{Cu-K}\alpha_1$  line from the emission tube. The sample is mounted on a stage having multiple degrees of freedom. This mobility of the sample stage helps to select diffraction from a specific crystal orientation. Valuable information can be gained by fixing the detector at the center of the expected Bragg reflection and following the diffracted intensity as the sample is independently rotated (or "rocked"). Such an arrangement for diffraction measurements

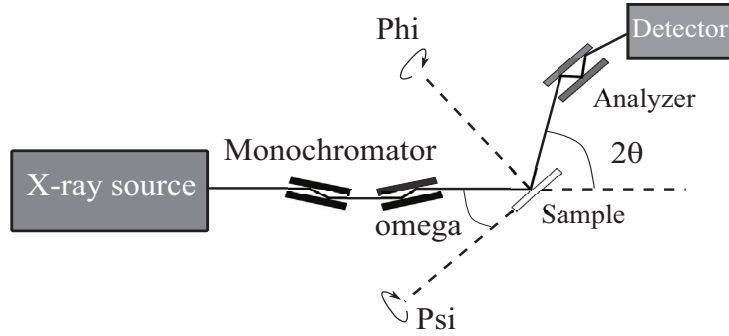


**Figure 4.4.** Simplified schematic illustration of the XRD setup.

is known as rocking curve mode.

XRD rocking curves have been extensively used to study the mosaic tilt and twist in imperfect GaN layers [66]. The tilt describes the out of growth plane rotation of mosaic blocks and is associated with the presence of screw-type TDs.  $\omega$ -scans of  $00l$  reflections can be used to estimate the lattice tilt arising from screw- and mixed-type dislocations. Twist is associated with the in-plane rotation of the mosaic structures and it is caused by the presence of edge- and mixed-type TDs.  $\omega$ -scans taken in off-axis rotations can be utilized to estimate the presence of twist [67, 68]. For the estimation of twist in our samples, the full width at half maximum (FWHM) of  $\omega$ -scans were measured from 302, 201 and 121 reflections [Publication I and II]. These reflections occur at higher angles and  $\omega$ -FWHM is dominated by an in-plane twist. Estimation of mosaic imperfections in GaN using these reflections have been reported previously as well [67].

For the MQW structures the  $\omega - 2\theta$  HRXRD scans were taken. A typical  $\omega - 2\theta$  consists of several distinct peaks. The highest intensity peak originates from the substrate or a thick underlying layer. Satellite peaks (zero- and higher-order) appear on either side of the substrate peak and can be a representative of the diffraction pattern of MQW stack. Apart from this several interference fringes due to different optical paths of X-rays are also present. The zero-order satellite peak can be used for a very rough estimation of composition of one repeat in MQW (barrier and well). The peak separation can be used for estimating period thickness. For a more accurate determination of layer thickness and composition the experimental and theoretical diffraction patterns must be simulated together by using complex algorithms [69]. Commercial simulation softwares use dynamical theory for analysing the diffraction data. While this approach

can be true for simple semiconductor heterostructures, the analysis of complex layered structure requires a combination of other measurement techniques together with XRD [70].

In this thesis, secondary ion mass spectroscopy (SIMS) was employed as an additional method to analyse the quaternary III-nitride structures. SIMS relies on the impact of energetic ions or neutral particles on the sample surface. This induces the release of ionized particles and they are characterized in a mass spectrometer. Since the material is removed from the sample during the SIMS measurements, it provides the possibility of achieving the depth profile of the surface [71]. For this work the SIMS data from quaternary III-nitride samples was used to aid in achieving a better fit between the XRD simulations and experiments.

#### 4.4 Luminescence spectroscopy

The process of carrier recombination in semiconductors usually results in photon generation. The transition of an electron from a higher energy state to a lower energy state results in the loss of energy and emission of a photon. This phenomenon is known as spontaneous emission. Luminescence in response to external excitation is one of the most interesting properties of direct band-gap semiconductors. This light emission can be triggered either by optical excitation or by electrical injection of carriers. The radiative recombination of carriers as a result of absorption of photons is termed as photoluminescence (PL). The information on the band gap of the semiconductor structures can be obtained by employing PL spectroscopy. PL spectroscopy is particularly attractive technique since it is fast, non-destructive and the measurement requires no sample preparation. The photons generated as a result of optical excitation are collected and analysed by a spectrometer.

In this thesis, the QWs were characterized by performing PL measurements at room temperature (RT) and at 10 K. The room temperature measurements in Publication V and VI were carried out by using excitation from a He-Cd laser with an emission wavelength of 325 nm. The maximum output power of this laser is 25 mW. An Ocean Optics USB2000 spectrometer was used as a detector. The low temperature (LT) PL measurements were used to further investigate the optical quality of InGa<sub>N</sub>/InAlGa<sub>N</sub> QW samples. An estimation of the internal quantum efficiency

(IQE) of the MQW structures was made by evaluating the integrated PL signal ratio at 300 K and 10 K [72, 73]. This method is based on the assumption that non-radiative recombination processes are not active at very low temperatures.

The light emission induced by electrical injection of charge carriers is known as electroluminescence (EL). To investigate the EL properties of GaN LEDs, several different types of metal contact schemes were used in this thesis. For quick EL measurements a  $0.5 \text{ mm}^2$  soldered metallic In droplets were used to make contacts on p- and n- layers on the LED wafers. For more detailed and accurate EL analysis the LED wafers were processed into square mesas having a dimension of  $440 \times 440 \text{ }\mu\text{m}^2$ . ICP-RIE was used to etch through the p-GaN and QW layers to expose the n-GaN surface for evaporation of the n-metal contact. A more detailed description for the different metal contact schemes is given in chapter 6 and 7. To analyse the performance of LED devices the output power and EL spectra were obtained from several individual chips.



## 5. III-N light emitting diodes (LEDs)

The first three sections of this chapter discuss the history, development and epitaxial structure of III-N LEDs. Section 5.4 discusses the challenges associated with the realization of highly efficient blue LEDs.

### 5.1 Overview

III-nitride compound semiconductors have already shown their importance in a number of applications including blue/UV LEDs and laser diodes (LDs), high power transistors and photodetectors [74, 75]. The performance of GaN-based blue LEDs improved drastically during the mid 90s after the successful demonstration by Nakamura [32]. Since then the GaN based LEDs and LDs have penetrated the consumer market. Efficient InGaN/GaN blue LEDs are used to excite a thin layer of yellow phosphors to extract white light out. Another approach is to use GaN-based UV LEDs to excite phosphors for creating white light. However, due to certain technological barriers the UV LED performance is not up to point where an efficient excitation of phosphors can take place. For this reason blue LEDs remain to be the primary choice for general illumination applications. The blue LEDs in the wavelength range of around 450 nm are being successfully employed for general lighting applications with the use of appropriate phosphor coating. The efficacy of GaN light sources demonstrated in recent years has already crossed 245 lm/W for white light [1]. Although GaN based LEDs are readily available commercially, there are still many challenges that need to be addressed. The non-availability of substrates, light extraction, green/yellow gap and efficiency droop are some of the key issues that are still considered to be the major challenges in the realization of highly efficient light emitting devices.

## 5.2 History of GaN-based LEDs

The first report of GaN growth dates back to 1969 when Maruska *et al.*, reportedly grew single crystal GaN on sapphire substrate by HVPE [39]. In 1971 Pankove *et al.*, reported on the fabrication of first blue LED having metal-insulator-semiconductor (MIS) structure [76]. Although this demonstration of blue light source is important historically, from the performance point of view the device was highly inefficient. Akasaki and his team worked on the MBE growth of GaN layers but it did not lead to any significant breakthrough [77]. The research and development nearly stalled for more than a decade after Pankove's discovery. This slow progress was associated with the difficulties in growing crack free smooth GaN layers and the inability of to achieve acceptable p-type conduction due the high levels of residual donor densities ( $> 10^{19} \text{ cm}^{-3}$ ).

In 1986 Amano and co workers reported the MOVPE growth of high quality single crystal GaN layers on sapphire by employing a low temperature AlN buffer layer. The buffer layer technique helped in the reduction of interfacial free energy caused by a large thermal and lattice mismatch between GaN and sapphire substrate. Later in 1991 Nakamura reported the growth of GaN layer by using a LT-GaN buffer layer. He reported carrier concentration and hall mobility of  $4 \times 10^{16} / \text{cm}^3$  and  $600 \text{ cm}^2 / \text{Vs}$ , respectively, at room temperature [41]. Nowadays the use of LT-buffer layer has become standard practice when growing GaN layers on sapphire.

The problem of poor crystalline quality was partially resolved after the adoption of the LT-buffer technique. This development brought the researchers one step closer towards realizing efficient III-N LEDs and LDs. The second major issue of p-type doping was solved again by Nakamura and co workers in 1992. They achieved high dopant concentration in p-type GaN layers with thermal annealing of the layers [78, 79]. Their reported values were even better than those of Akasaki *et al.*, who had previously used electron beam irradiation to increase the p-type conductivity in GaN layers. It is now a well established fact that thermal annealing helps in the activation of Mg acceptors that are passivated by hydrogen during MOVPE growth.

The GaN based light emitting devices have come a long way since Nakamura's groundbreaking work in the early 90's. Thanks to many technological advancements, the overall efficiency of GaN blue LEDs has improved considerably over last few years [80, 81]. Phosphor coated blue LEDs are

currently being used to generate white light. Technology for white LEDs based on phosphor conversion has matured into a multi-billion dollar industry and is considered as a strong contender for next generation lighting applications. InGaN/GaN LEDs operating close to the well known green/yellow gap *i.e.*, 530 - 590 nm of wavelength still suffer from poor efficiencies. The reason for this is the high percentage of indium required in the QWs to achieve longer wavelengths. Increasing the indium fraction in InGaN QWs to more than 20 % leads to a higher number of defects. Furthermore, the incorporation of In is limited due to compositional pulling effect that is caused by the large lattice mismatch between GaN and InGaN [82].

### 5.3 Epitaxial structure of blue and near UV LEDs

Due to the non-availability of cheap inexpensive GaN substrates, the epitaxial structure starts usually with the growth of a GaN buffer layer on a sapphire substrate. Even when grown with the two step method, GaN buffer layers usually possess high density of defects which originate from the large lattice mismatch between the substrate and the epitaxial layer. Several ideas have been proposed and successfully employed to reduce the defect density, details of which will be discussed in the next chapter. To continue this discussion on the epitaxial structure it is very reasonable to say that the atomically flat surface of a GaN buffer layer serves as a starting point for the growth of actual device layers in an LED.

The buffer layer is followed by a n-doped GaN layer. MOVPE grown non-doped GaN is typically n-type. This intrinsic n-type behavior is attributed to the presence of residual impurities like Si and O [83]. In order to intentionally n-dope GaN, silicon is the element of choice which has been widely used. The controllable range of n-type doping has been shown to be between  $5 \times 10^{16} - 5 \times 10^{19} \text{ cm}^{-3}$  [84].

The MQW stack is placed between the n- and p-type layers. MQW stack typically consists of InGaN wells and GaN barriers. Light generation takes place inside the QWs. The emission wavelength depends on the percentage of indium and the thickness of QWs [85]. Growth of InGaN QWs and GaN barriers is particularly challenging since there is a very narrow growth window available to operate during their epitaxial growth. The situation becomes even more challenging when quaternary layer is

involved in the MQW stack [ Publication V and VI]. This topic will be further discussed in the next chapter. The growth of MQW stack is usually followed by a thin Mg-doped AlGa<sub>N</sub> layer [86, 87]. This large band gap layer is often referred to as the electron blocking layer (EBL). The purpose of the p-doped AlGa<sub>N</sub> layer is to suppress the electron overflow to the p-side and to ensure that the recombination of electrons and holes takes place in the active region. The EBL layer is followed by the growth of a p-GaN layer which is the final epitaxial layer in a GaN based LED. The epitaxial structure is then in-situ annealed at temperatures in excess of 600 °C in N<sub>2</sub> ambient for passivation of hydrogen in p-GaN layer.

Some compositional changes in the device layers can help in fabricating near UV LEDs (370-400 nm). In order to shift the emission peak of the QWs below 400 nm, a lower indium content and thinner wells are critical requirement. Along with this, AlGa<sub>N</sub> or InAlGa<sub>N</sub> barriers are also required in order to ensure sufficient carrier confinement [88]. A careful optimization of composition for the barrier layers can help in growing lattice matched QW and barrier layers.

## 5.4 Challenges for GaN based LEDs

Although the improvement in the performance of III-N LEDs has shown a positive trend, there are still many challenges that need to be addressed. The issues such as the lack of native substrates, polarization fields, efficiency droop and light extraction are some of the extensively studied topics on GaN in recent years. The use of foreign substrates is directly associated with the mismatch in thermal expansion coefficient and lattice constants, thus, resulting in high concentration of defects [89]. Although a high density of dislocations does not influence the device operation too much at low current density, the situation gets worse for high currents [90]. Polarization fields have a strong impact on device performance when the crystals are grown in [0001] direction.

Efficiency droop in III-N LEDs means a reduction of efficiency with increasing injection currents. The origin of efficiency droop is still not fully understood. Several mechanisms including recombination at dislocations, carrier leakage and Auger recombination have been suggested to explain the droop in GaN LEDs [91, 92]. Some of the key approaches that look promising in reducing the efficiency droop are charge polarization match-

ing of layers with the nitride material, using thicker QWs and altering the device structure to reduce carrier overflow [93, 94, 95].

The next big issue for the modern day LEDs is the enhancement of EQE. EQE is a product of IQE and light extraction efficiency (LEE). Rapid development of various growth techniques and epitaxial structures has already boosted the IQE of GaN-based LEDs to more than 80 % [96]. On the other hand, the LEE from a conventional LED structure is still quite low. If we assume that light emitted from sidewalls and backside is not utilized, one expects that approximately only 4% of the internal light can be extracted from a surface [97]. The reason for this low value is large difference in the refractive indexes of GaN ( $n \approx 2.5$ ) and air ( $n \approx 1$ ). An absorbent substrate, non-transparent ohmic contacts to the device and total internal reflection (TIR) are the main causes for reduced LEE in conventional III-N LEDs. Several proposed techniques like flip-chip [98], transparent conducting layers and their patterning [99], surface roughening [100], using of photonic crystals [101], patterned sapphire substrates [102], sidewall etching of GaN chips [103], creation of voids at GaN-sapphire interface [104] etc. have been successfully employed to overcome the shortcomings related to poor light extraction. This thesis also proposes different methods of improving light extraction. A novel method for enhancing light extraction along with improved crystalline quality has been proposed [Publication I, II and III]. The details associated to this method are discussed in the next chapter.



## 6. Light extraction techniques and quaternary nitride structures

This chapter reviews the details associated with MOVPE growth and characterization of III-N layers that were fabricated for this research work. The chapter starts with a background discussion of various techniques that have been used over the years to improve the performance of GaN based devices. The next two sections include a discussion on two different approaches that were used to improve the total light output from the LED structures grown on sapphire substrates. The last section highlights the issues involved in growth of quaternary InAlGa<sub>N</sub> layers.

### 6.1 Shape controlled voids in pendeo epitaxial GaN

In recent years, there has been an increased interest towards selective area growth of GaN through highly defined patterns on GaN templates [105, 106]. Void generation has been reported in many different kinds of lateral overgrowth techniques, be it the lateral overgrowth of nanocolumns [107, 108], pendeo epitaxy (PE) or epitaxial lateral overgrowth (ELOG) [109]. On the one hand it has been argued that the formation of voids plays a key role in stress relaxation, crack suppression and reduction of TD density [110], while on the other hand voids can help in effectively diffracting light into the escape-cone and, thus, increasing the escape probability in light emitting structures [111]. Furthermore, the presence of voids can also assist in the lift-off process for the removal of substrates [112, 113].

The TD density in GaN grown on sapphire is several orders of magnitude higher compared to other compound semiconductor materials. Formations of TDs at the coalescence boundaries or at the defect sites near GaN/sapphire interface are the two most widely accepted mechanisms behind high TD densities. Despite a large number of TDs present in GaN,

the GaN based LED devices show much lower sensitivity to TDs compared to LEDs fabricated from other III-V or II-VI compounds. On the other hand GaN based lasers and high frequency transistors are far more sensitive to the TD density in GaN layers compared to GaN LED operating in blue wavelength regime. Over the years, several in-situ and ex-situ methods have been proposed to reduce the TD density in GaN layers. In-situ methods may include nitridation of sapphire, AlN or GaN nucleation layer, insertion of SiN interlayer or a combination of these techniques etc. Ex-situ methods may include ELOG (1-step ELOG or 2 step ELOG, maskless ELOG), facet controlled lateral overgrowth (FACELO), PE etc [114]. The TD reduction in many of these methods is achieved by changing or blocking the propagation trajectory of TDs. In some methods a combination of both of these mechanisms are utilized.

This section elaborates a part of this research work where the focus was to intentionally create voids inside epitaxial GaN layers at the GaN-sapphire interface. Epitaxial growth of GaN LEDs on GaN templates having hexagonal openings can provide two-fold benefit, *i.e.*, improved material quality by TD bending and enhanced light extraction. The proposed method is different from conventional ELOG or PE where stripe patterns are used. Such kind of lateral growth on patterned stripes is much more suitable for laser diodes where the device can be fabricated in the low TD density stripe area. The details to follow elaborate the fabrication of GaN templates with hexagonal openings, MOVPE growth of GaN on such templates, void generation and their shape control, structural analysis of GaN layers with voids and the influence of voids on LED device performance. The lateral growth on GaN templates with periodically arranged openings can result into comparatively more homogeneous distribution of TD density.

C-plane epi-ready sapphire substrates were used as a starting point to grow GaN layers in a MOVPE reactor system. The conventional two step process as mentioned in Chapter 3 was used to grow 3.2  $\mu\text{m}$  thick GaN layers. The growth was stopped and the samples were taken out of the MOVPE reactor. Hexagonal photoresist patterns having diameters of 2, 3 and 4.5  $\mu\text{m}$  were fabricated by using a standard photolithographic process. The hexagonal patterns were not aligned to any specific crystal orientation. An e-beam metallization tool was used to evaporate Ni onto these structures. This was followed by a lift-off process in an ultrasonic bath. The next step was to etch the GaN layer through the hexag-

onal openings with Ni as a mask layer. The samples were etched in an ICP-RIE chamber.  $\text{Cl}_2/\text{Ar}$  based plasma process was used for the etching of GaN from the un-masked areas. The samples were etched down to GaN-sapphire interface. The purpose of this step was to remove the 0001 GaN surface from the hexagonal openings. Fig. 6.1 shows tilted view and cross-sectional SEM images of GaN templates after the ICP-RIE process. Hexagonal openings with a diameter of 2 and 3  $\mu\text{m}$  are shown in Fig. 6.1a and 6.1b, respectively.

Aqua regia solution was used to remove the Ni metal after the dry etch process. The samples were then cleaned with acetone, 2-propanol, piranha etchant, buffered HF mixture and finally rinsed with DI water before drying. The sample preparation and cleaning procedure as mentioned above were used as a standard for all of the samples that underwent MOVPE regrowth process.

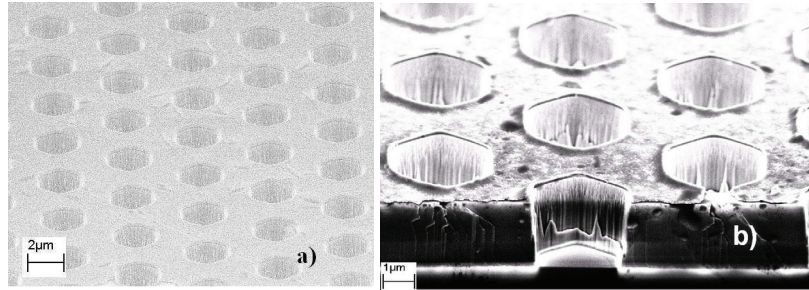


**Figure 6.1.** Tilted view SEM images of 3.2  $\mu\text{m}$  deep ICP-RIE etched GaN templates with different diameter of hexagonal openings: (a) 2  $\mu\text{m}$  and (b) 3  $\mu\text{m}$  [Publication 1].

To investigate the GaN regrowth behavior, the samples with the opening diameter of 4.5  $\mu\text{m}$  were selected for initial experiments. The GaN regrowth process was carried out at 1030  $^{\circ}\text{C}$  with different  $\text{NH}_3$  partial pressures inside the MOVPE reactor for 4000 sec. Fig. 6.2a shows the side view cross-sectional SEM image of the sample grown with a V/III ratio of 720. We observe the formation of V-shaped hexagonal pits that rise to the top of the surface from inside the hexagonal openings. The SEM images suggest that the V/III ratio of 720 leads to a slow lateral and high vertical growth rate of GaN. This eventually results in an incomplete coalescence of the grown layer as observed in the top view SEM image in Fig. 6.2b. The cross-sectional SEM image in Fig. 6.2c shows the sample grown with a V/III ratio of 1440. The sample grown with such a high V/III ratio shows complete coalescence of the hexagonal openings. Increasing the V/III ra-

tio has been shown to enhance the lateral growth rate of GaN. This is due to the fact that high V/III ratio increases the surface active nitrogen concentration, which eventually increases the incorporation probability of Ga atoms [115].

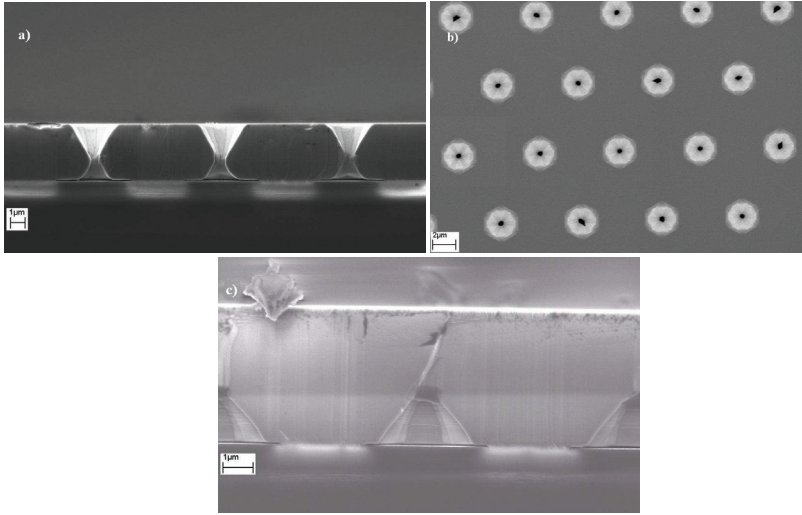


**Figure 6.2.** SEM images of GaN layers grown on patterned GaN templates at 1030 °C for 4000 sec: (a) and (b) V/III ratio of 720 (cross-sectional and top view); (c) V/III ratio of 1440 (cross-sectional view) [Publication I ].

Fig. 6.3a, 6.4a and 6.5a show the side view cross-sectional SEM images of three simultaneously regrown GaN templates with an initial thickness of 3.2 μm. Hexagonal openings with different diameters (2, 3 and 4.5 μm) were etched into these GaN templates. The black colored dashed lines depict the location of ICP-RIE etched GaN openings prior to the regrowth step. The samples were grown at a temperature of 1030 °C with a V/III ratio of 1440.

The sample with the opening diameter of 2 μm (Fig. 6.3a) shows sidewalls with an inclination angle of 85° after the complete coalescence is achieved. The bottom and top-most portions of the void sidewalls in Fig. 6.3a have higher inclination as compared to the central portion of the sidewall. The inclination angle value of 85° in Fig. 6.3a is estimated from the large central portion of the void side walls. Fig. 6.3b shows a cross-sectional bright field TEM image of the same sample with a close-up view of the edge of the void's sidewall. It can be observed from Fig. 6.3b, that most of the TDs propagate upwards away from the interface. The free surface of the void does not influence the trajectory of TDs.

The voids formed as a result of GaN regrowth on GaN template with an

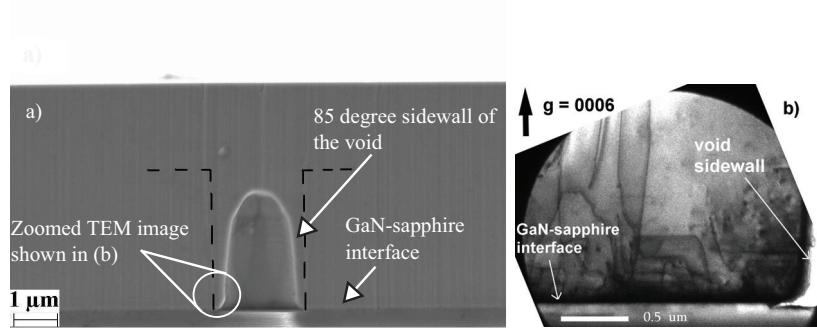


**Figure 6.3.** (a) Cross-sectional SEM image of a void in a regrown GaN layer with a side wall inclination angle of 85° and (b) close-up bright field TEM image of void sidewall near GaN-sapphire interface [Publication I and II].

opening diameter of 4.5 μm is shown in Fig. 6.4. An inclination angle of around 60° can be seen from the void sidewall. Fig. 6.4b shows a cross-sectional bright field TEM image of the same sample with a close-up view of the edge of the void's sidewall. A large number of threading dislocations originate from the GaN-sapphire interface and they propagate away from this interface. An important observation from Fig. 6.4b is that many of these TDs undergo a perpendicular re-orientation in their propagation trajectory. The perpendicularly bent threading dislocations have been marked as PBTD in Fig. 6.4b. After the perpendicular re-orientation in their propagation trajectory, these TDs terminate at the inclined sidewall of the void.

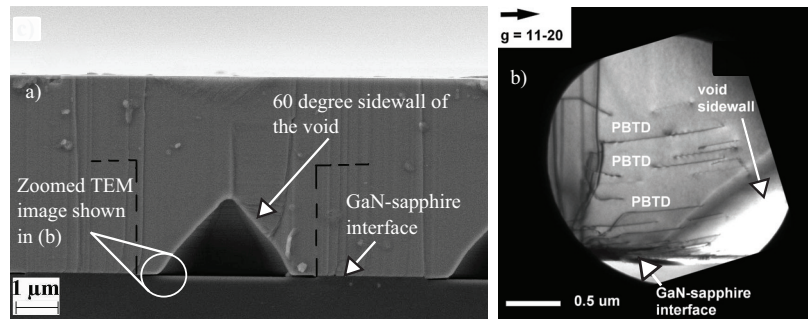
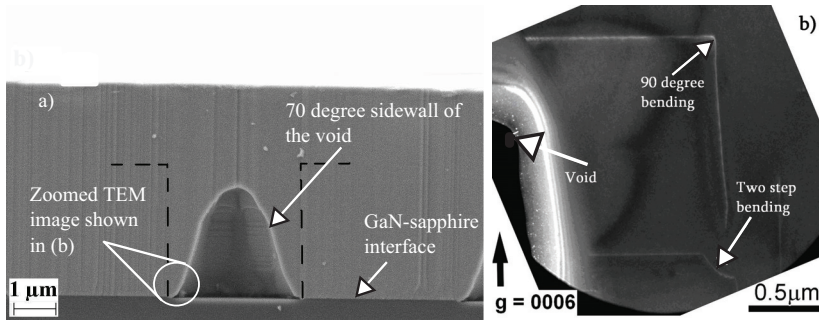


**Figure 6.4.** (a) Cross-sectional SEM image of a void in a regrown GaN layer with a side wall inclination angle of 60° and (b) close-up bright field TEM image of void sidewall near GaN-sapphire interface [Publication I and II].

The voids in the sample in Fig. 6.5a which had an opening diameter of 3 μm before the regrowth show an inclination angle of 70°. The bottom and top-most portions of the void sidewalls in Fig. 6.5a have higher inclination compared to the central portion of the sidewall. The inclination angle value mentioned for Fig. 6.5a is estimated from the large central portion

of the void sidewalls. Fig. 6.5b shows the cross-sectional dark field TEM image of dislocations bending near the void. One of the dislocations propagates towards void sidewall through a single step perpendicular bending. This threading dislocation shows a sharp bending angle of  $90^\circ$ . Another threading dislocation marked in Fig. 6.5b undergoes a change in the dislocation line trajectory through multi-step bending. An angle of  $47^\circ$  is observed from the large central portion of the TD that bends in two steps. It has been proposed that the TDs that bend in several steps pass through the local energy minimum before bending towards the energetically most stable direction [116].

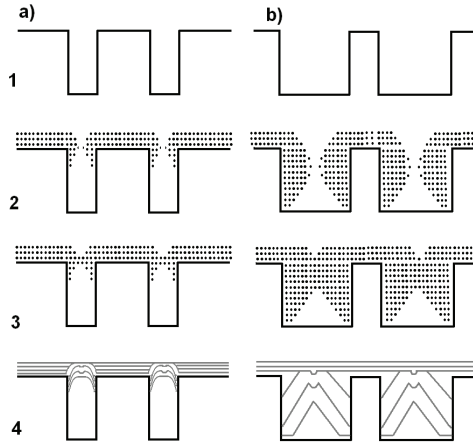
Our results have shown that the sidewall angle of the voids after the regrowth process is most likely not a function of the orientation of the etched face of the individual hexagonal side wall. Since the sidewalls of initially etched hexagons (as shown in Fig. 6.1) did not necessarily correspond to any particular crystal plane of the GaN lattice, we believe that the formation of nearly vertical or inclined walled voids is a strong function of the geometrical dimensions of hexagonal openings.



**Figure 6.5.** (a) Cross-sectional SEM image of a void in a regrown GaN layer with a sidewall angle of  $70^\circ$  and (b) close-up dark field TEM image of void sidewall near GaN-sapphire interface [Publication I and II].

To illustrate the regrowth process, the schematics in Fig. 6.6 show the proposed model for GaN regrowth. Fig. 6.6a describes the regrowth steps in the case of a sample which has etched structures with a small opening diameter. There is a large difference in the supply of the reactive species at the top of the sidewalls compared to the bottom of the hexagonal opening. The domination of diffusion limited regrowth process favors the growth of the top-most area both vertically and sideways. Such diffusion limited process has been previously modeled by H.J. Oh *et al.*, [117]. As the structure continues to grow both vertically and horizontally the opening starts getting smaller from the top. It becomes more and more

difficult for the atoms to diffuse down to the bottom of the etched opening and deposit on the sidewalls. This eventually results in a minimal growth on the sidewalls of the opening.



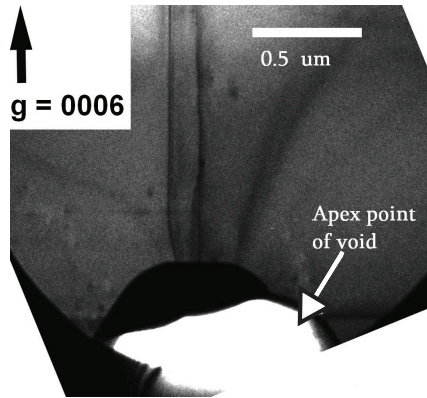
**Figure 6.6.** Proposed model of regrowth mechanism with etched structures of: a) small opening diameter; b) large opening diameter [Publication I].

Fig. 6.6b shows the case with a large opening diameter of the etched structures. The larger opening size leads to a higher concentration of source materials at the bottom of the opening. A local gradient of III and V species is created along the sidewalls inside the hexagonal opening with a large diameter. This gradient of reactive species is formed due to the depletion of gas phase of the molecules that are incorporated into the growing layer. This depletion is compensated by diffusion of growth species from the gas phase. As the growth continues, the opening gets narrower. This narrowing limits the diffusion of growth species to the bottom of the opening. The proposed growth model is supported by the experimental observations according to which the opening diameter of the etched hexagonal patterns in GaN plays a key role in the final evolution of the shape of the voids that remain embedded at the GaN-sapphire interface.

It is well known that as a result of lateral epitaxy new dislocations can be generated at the meeting point of two growth fronts [118]. We have observed a similar sort of behavior in our samples as seen in Fig. 6.7 which shows a bright field TEM image of the apex point of a void. The crystallographic misorientation of the meeting fronts at the apex point results in the formation of TDs.

The results presented so far show that the epitaxial growth process on the patterned GaN templates changes with varying size of hexagonal

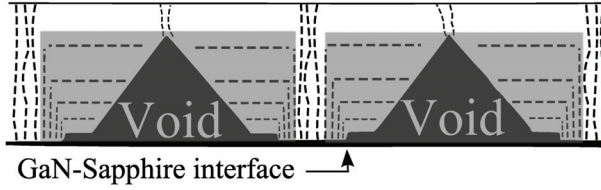
openings [Publication I]. The kind of growth mode also has an effect on the TD line trajectory. TD bending is well documented phenomenon for different lateral epitaxial techniques such as FACELO, ELOG or PE [113, 119, 120, 121]. Despite some minute differences between these processes, dislocation reduction is achieved by common mechanisms, *i.e.*, primarily by mask blocking and/or dislocation bending. However, the exact reason behind TD bending is still not fully understood. Reduction in elastic energy of the TD or the role of image forces on TD are the two most commonly mentioned explanations for TD bending [122, 114].



**Figure 6.7.** Bright field TEM image of the coalescence point on top of the void [Publication II].

Based on our experimental TEM observations of TD propagation in such structures, we have established a model that explains the movement of TDs. Fig. 6.8 shows two schematics for the two cases of TD propagation that are based on two different opening sizes resulting in the formation of voids having different shapes. After comparing the dislocation bending phenomenon as observed in samples having different opening sizes, we propose that the geometry of the area where the regrowth takes place not only governs the regrowth process but also influences the trajectory of dislocation lines near the free surfaces. In the case of model A, the amount of void free surfaces available to interact with the strain field of dislocations is large. Such a scenario accounts for significant lateral growth and a stronger interaction of dislocations with the large openings and, thus, results in bending of TDs that are located at different distances from the free surface. In the case of Model B the decreased opening size limits lateral growth of material and the screening of strain fields by the free surfaces is not so strong and, thus, no noticeable amount of dislocations bend towards the free surface.

## Model - A



## Model - B

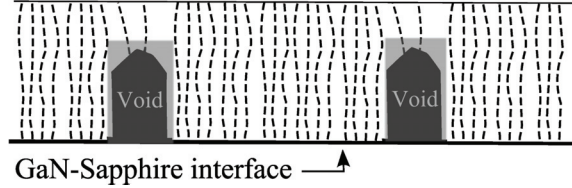


**Figure 6.8.** Schematic illustration of threading dislocation trajectory near void's side-walls with: Large opening size resulting in Model-A and small opening size resulting in Model-B. The grey area shows the original etched openings prior to regrowth [modified from Publication II].

Table 6.1 shows the results of experimentally measured values from XRD measurements. The FWHM values of  $\omega$ -scans for the two samples having different void shapes at different diffraction reflections were measured. A reduction in the FWHM values of the  $hkl$  scans in the sample with the initial opening diameter of  $4.5\ \mu\text{m}$  is observed. These results point towards the reduction of screw- and mixed-type threading dislocations in the sample [Publication II and III]. Comparing the  $\omega$ -FWHM of 201 and 121 rocking curves, we observe a significant drop in values for larger opening diameter samples. Backed by our TEM investigations, we conclude that there is reduction in edge- and mixed-type dislocations in the sample grown on GaN template having an opening diameter of  $4.5\ \mu\text{m}$ .

**Table 6.1.** FWHM values of  $\omega$  rocking curves obtained from different  $hkl$  reflections [Publication II].

	reference sample	opening diameter 2 $\mu\text{m}$	opening diameter 4.5 $\mu\text{m}$
FWHM <sub>002</sub> (arcsec)	280	260	180
FWHM <sub>201</sub> (arcsec)	630	590	250
FWHM <sub>121</sub> (arcsec)	610	610	240

To test the effect of voids in general and the void geometry in particular, InGaN/GaN based LED structures with an emission wavelength of 405 nm were grown on GaN layers with embedded voids. Fig. 6.9 shows a

3D artistic view of a fully processed LED structure with voids embedded at the GaN-sapphire interface. Ti/Al/Ti/Au metal scheme was used as n- and p-metal contacts. A transparent conducting oxide (TCO) layer was used on entire p-GaN area for efficient current spreading. The inset (a) in Fig. 6.9 shows the top view optical image of such an LED chip. The image was taken near the n-metal contact and focused in such a way that the embedded voids were visible. The inset (b) in the same figure shows the cross-sectional SEM image of voids having a sidewall inclination angle of  $70^\circ$ .

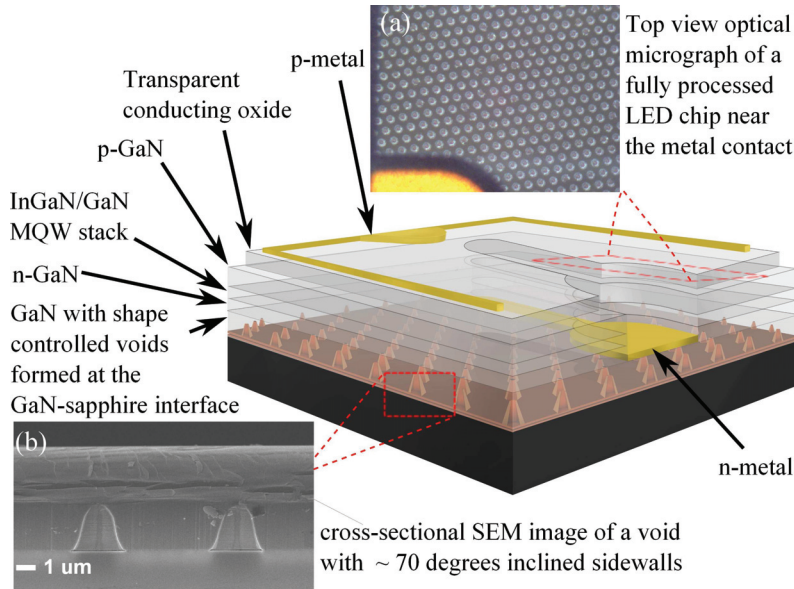


**Figure 6.9.** 3D artistic view of a fully processed LED chip with embedded voids at the GaN-sapphire interface. Inset (a) showing the optical micrograph of an LED chip with embedded voids in focus. Inset (b) showing the cross-sectional SEM image of the void at the GaN-sapphire interface having an inclined sidewall angle of  $70^\circ$  [ Publication III].

Individual LED chips were bonded onto TO-headers. An integrating sphere was used for the EL measurements. The Fig. 6.10 shows the light output characteristics of  $\sim 85^\circ$  and  $\sim 60^\circ$  inclined sidewall void structures along with the reference LED without voids. At 20 mA current injection, the reference LED gives 9.4 mW light output. It can be seen from the Fig. 6.10 that introducing the  $\sim 85^\circ$  and  $\sim 60^\circ$  inclined sidewall voids at the GaN-sapphire interface enhances the light output to 10.2 and 11.4 mW at 20 mA, respectively.

It is evident from the results that the void geometry can be controlled through appropriate selection of initial pattern shape and dimensions.

Fine tuning of the voids can make it an efficient light scattering object and, thus, enhance the light extraction efficiency of LEDs. At the moment the authors are convinced that the enhanced light extraction is playing a dominant role in increasing the light output of embedded void LED structures. Further investigations are necessary to quantify the role of template structure quality and its impact on IQE of such LED structures.

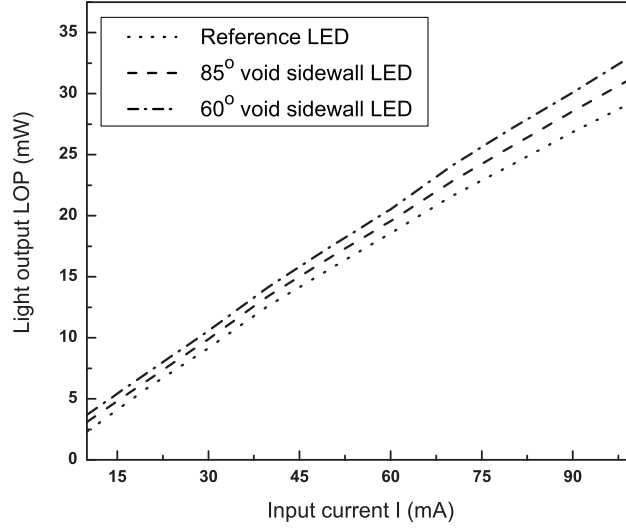


**Figure 6.10.** Light output characteristics of LEDs grown on templates with  $\sim 85^\circ$  and  $\sim 60^\circ$  void sidewall angles together with a reference LED.[ Publication III].

## 6.2 Maskless sapphire roughening

The experimental investigation on the wet etching of sapphire substrates was carried out in two parts. In the first part, the effect of etching mixture on sapphire was tested. In the second part, the back side of the sapphire substrate surface was wet etched after the epitaxial growth of an LED structure and its effect on the LED device performance was evaluated.

To start our investigation, we covered the front side of 430  $\mu\text{m}$  thick (0001) sapphire samples with a 300 nm thick  $\text{SiO}_2$  by using plasma enhanced chemical vapor deposition (PECVD). Then the  $\text{SiO}_2$  etching mask was patterned on the sapphire surface. To determine the role of the etching mixture on the etching rate and the surface quality, the samples were etched at around 300  $^\circ\text{C}$  for 10 min in an acid mixture of  $\text{H}_2\text{SO}_4:\text{H}_3\text{PO}_4$  with the

ratio of 3:1. Fig. 6.11a shows a tilted view SEM image of a mesa structure on the sapphire surface etched with the  $\text{H}_2\text{SO}_4:\text{H}_3\text{PO}_4$  ratio of 3:1. This type of wet etching solution offered a very smooth and uniformly etched surface.

The SEM images in Fig. 6.11b and 6.11c show that four sided pyramid structures are created on the sapphire surface when pure  $\text{H}_2\text{SO}_4$  is used. A remarkable role of the redeposition can be seen from Fig. 6.11b where the redeposited material appears also on top of the  $\text{SiO}_2$  etching mask [Publication IV]. .

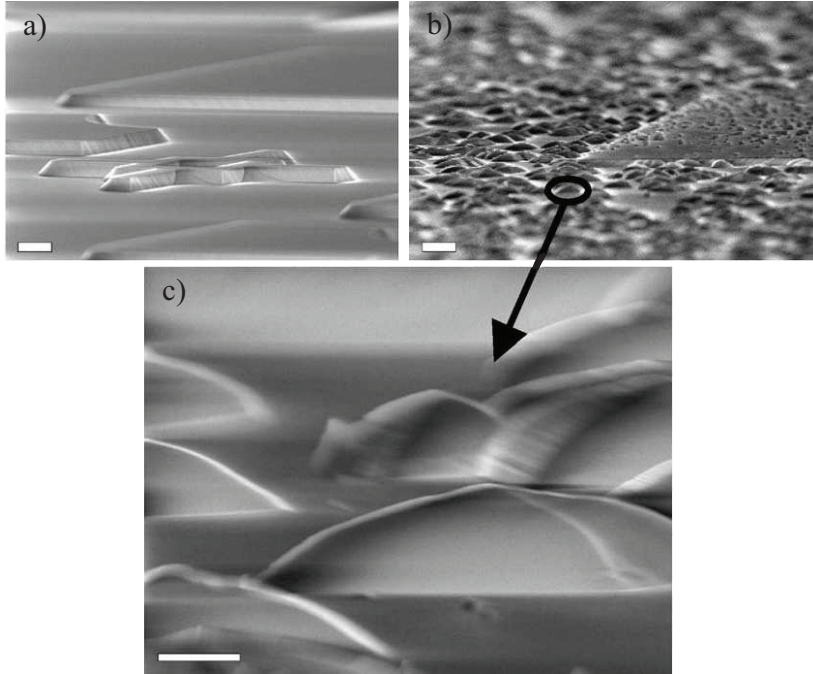


**Figure 6.11.** SEM images from the c-plane epi-ready sapphire surface after wet etching. It can be clearly seen from image (a) that etching mixture of  $\text{H}_2\text{SO}_4$  and  $\text{H}_3\text{PO}_4$  offers a smooth etched surface. Images (b) and (c) show that in the case of pure  $\text{H}_2\text{SO}_4$  etchant there is material redeposition and a strong crystal dependence of the etching. Image (b) shows also the redeposited material on the  $\text{SiO}_2$  mask. The scale bars correspond to 10  $\mu\text{m}$  in (a) and (b) and to 2  $\mu\text{m}$  in (c) [Publication IV].

The formation of four sided pyramidal shaped structure has already been reported by other groups as well [123]. According to literature the etching of sapphire in pure  $\text{H}_2\text{SO}_4$  leads to the formation of massive cubic etching product phase [124, 125]. The etching product phase can act as an etch mask during subsequent sapphire etching process. It has been confirmed by previous studies that the four sided pyramidal structures belong to the sapphire phase [125]. No etching reaction product is formed with the

addition of  $\text{H}_3\text{PO}_4$  to  $\text{H}_2\text{SO}_4$ . It implies that  $\text{H}_3\text{PO}_4$  has the etching capability for the reaction products formed in this process. This is in line with our experiments where we observed a smooth surface when  $\text{H}_2\text{SO}_4:\text{H}_3\text{PO}_4$  with the ratio of 3:1 was used as an etching mixture (Fig. 6.11a).

A set of non-patterned sapphire substrates were treated in pure  $\text{H}_2\text{SO}_4$  at  $300^\circ\text{C}$  for 5, 15 and 60 min. Fig. 6.12 shows the tilted view SEM images of the reference and the etched samples. The scattering objects were formed on the back side of sapphire and can be seen in Fig. 6.12b, c and d. It is evident from the SEM images that the size of the scattering objects can be tuned and modified by varying the etching time.

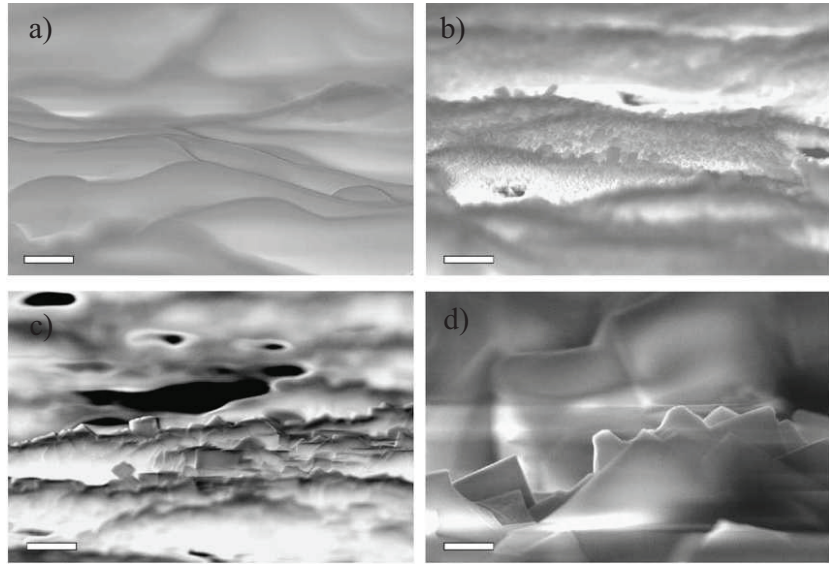


**Figure 6.12.** SEM images of the non polished sapphire backsides after  $\text{H}_2\text{SO}_4$  roughening of (a) 0 min, (b) 5 min, (c) 15 min and (d) 60 min. It can be seen that the size of the scattering cubic sapphire objects can be controlled with the etching time. The scale bars correspond to  $1\ \mu\text{m}$  [ Publication IV].

Two LED wafers from the same MOVPE run were selected to test the effect of back side roughening on the light output. Fig. 6.13 shows the EL results from a conventional non-roughened and a back side roughened LED wafer. The measured LED wafers were mounted directly on top of the integrating sphere for collecting the light extracted from the sapphire side of the LED structure. The backside roughened wafer gives 20-25 % higher light output compared to reference LED. The results present an evidence that hot  $\text{H}_2\text{SO}_4$  treatment of sapphire backside creates the light scattering structures and, thus, enhances the LEE from the LED wafers [ Publication IV]. This wet etching method can also be adopted for flip chip

LEDs where light is extracted from the back surface [126].

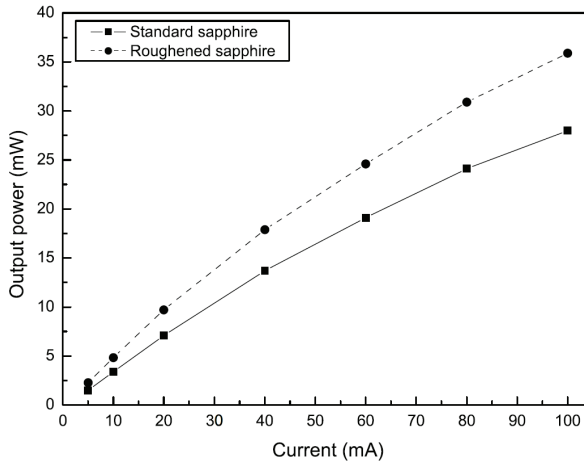


**Figure 6.13.** EL output power as a function of injection current. The plot clearly shows the increased EL output of the LED on the roughened sapphire [ Publication IV].

### 6.3 Quaternary nitrides for near UV emission

Efficient light sources operating at UV wavelengths are required for a number of applications, including lighting, sterilization, water purification, bio-medical and bio-chemical processes and for high density optical data storage [127]. AlGaIn material system is considered to be promising in UV-emitters since the energy band gap can be adjusted between 6.2 (AlN) and 3.4 eV (GaIn). However, due to the large dislocation densities in AlGaIn layers it is still difficult to fabricate a high efficiency UV light source [128]. A combination of InGaIn wells and GaIn barriers can also be used for near-UV emission but the weak carrier confinement significantly reduces the carrier localization [129]. High efficiency UV-emitters can be realized by using quaternary InAlGaIn layers. The InAlGaIn alloy system provides the flexibility of independent tuning of the band gap and the lattice constant. Furthermore, using quaternary alloy as a barrier layer allows the lattice strain of active InGaIn layer to be varied between compressive, tensile and zero [130, 131].

Several samples were prepared in order to investigate the growth conditions and properties of quaternary InAlGaIn layers. The quaternary layers were grown on a GaIn buffer layer at the temperature of 850 °C in nitrogen atmosphere with the reactor pressure of 300 Torr. Constant

flows of 25  $\mu\text{mol/min}$  and 51  $\mu\text{mol/min}$  for TMGa and TMAI, respectively, were used during growth. The V/III ratio was kept constant at 1100. The TMIn flow was varied in the range of 0-46  $\mu\text{mol/min}$ . Fig. 6.14 shows the HRXRD (002)  $\omega - 2\theta$  scans from a series of roughly 100 nm thick InAlGaN layers with different TMIn flows.

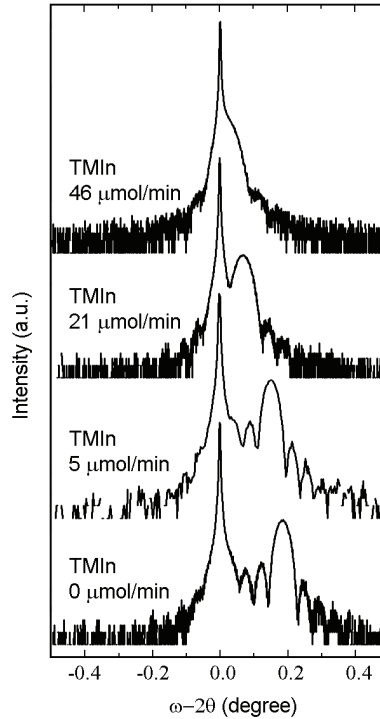


**Figure 6.14.** HRXRD ( $\omega - 2\theta$ ) curves of the (0002) reflection from InAlGaN films grown with various TMIn flows [ Publication V].

The results show that as the TMIn flow is increased, the InAlGaN diffraction peak shifts from AlGaN peak towards the GaN peak. The InAlGaN layer is almost lattice matched to GaN with TMIn flow of 46  $\mu\text{mol/min}$ . The full width at half maxima (FWHM) of the InAlGaN peak varies from 130 to 160 arcsec and is determined by the layer thickness. To evaluate the In and Al composition of the films, first Al content was measured by HRXRD from the sample grown with TMIn flow of 0  $\mu\text{mol/min}$ . 6.15 shows the In and Al content as a function of TMIn flow. It can be seen that TMIn flow has an effect on both the In and Al content of the films. The In content of the films increases and the Al content decreases with increasing TMIn flow. The Al content of the film grown with 46  $\mu\text{mol/min}$  was reduced by 40 % compared to the reference sample grown with 0 sccm of TMIn. The decrease in the Al content can partly result from the reduc-

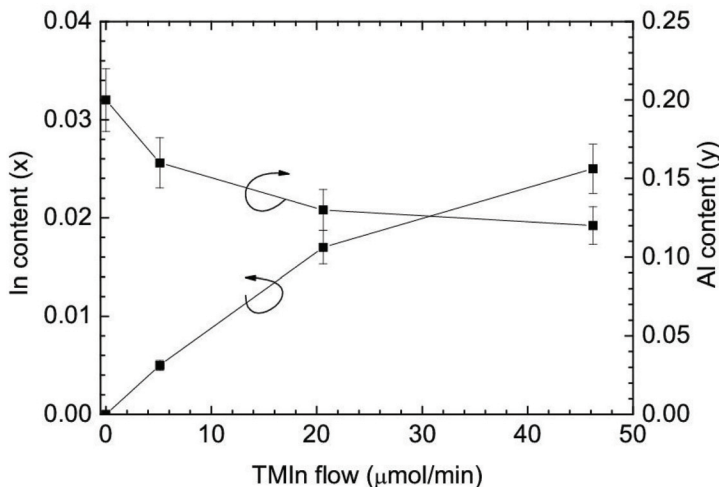


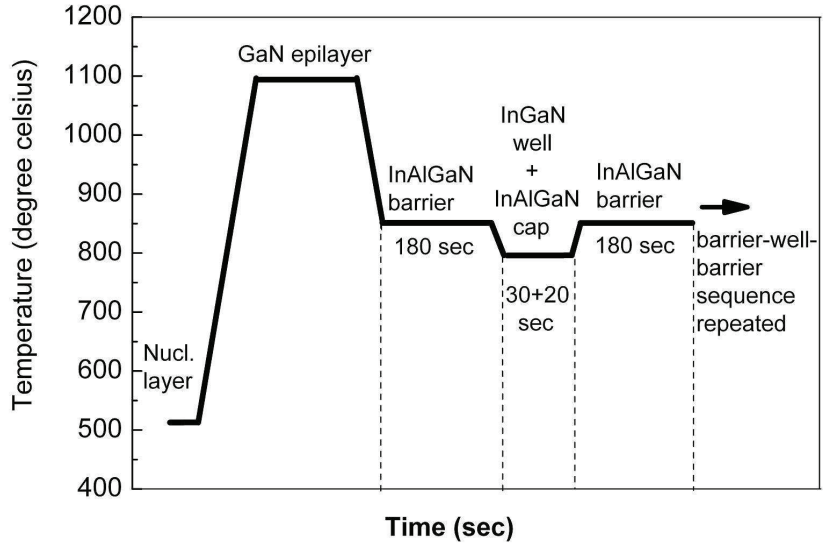
**Figure 6.15.** The In and Al contents of InAlGaN films as a function of TMIn flow [Publication V].

tion of the growth rate of the film. We observed that the growth rate of InAlGaN film decreased from 0.11 to 0.08 nm/s when the TMIn flow is increased [Publication V]. In the MOVPE growth of AlGaIn films reducing growth rate has been reported to decrease the Al content [132].

A series of InGaIn/InAlGaIn MQW structures emitting near 380 nm were fabricated to study the effect of barrier composition on the optical properties of QWs. The growth process flow is shown in Fig. 6.16. The MQW structure was grown on a 2 μm thick GaN buffer layer. After growth of the buffer layer the carrier gas was switched from H<sub>2</sub> to N<sub>2</sub>. The 2 nm thick InGaIn wells were grown at the temperature of 794 °C with a the growth time of 30 sec. After the growth of the InGaIn layer, a 2 nm InAlGaIn capping layer was grown at the same temperature. The capping layers were used to protect the active layer from the high temperature required for the growth of barriers with high crystalline quality. The temperature was then increased to 850 °C for 180 sec for the growth 20 nm thick InAlGaIn barrier layer. The whole sequence was repeated five times.

During growth of the barrier layers the TMGa flow of 25 μmol/min and the TMAI flow of 51 μmol/min were used. The TMIn flow was varied from 2.5 to 46.2 μmol/min during barrier growth. The precursor flows and the corresponding In and Al contents of the barriers are shown in table 6.2. The In and Al compositions in the barriers were estimated from a combination

of HRXRD (experimental and simulation data) and SIMS measurements.



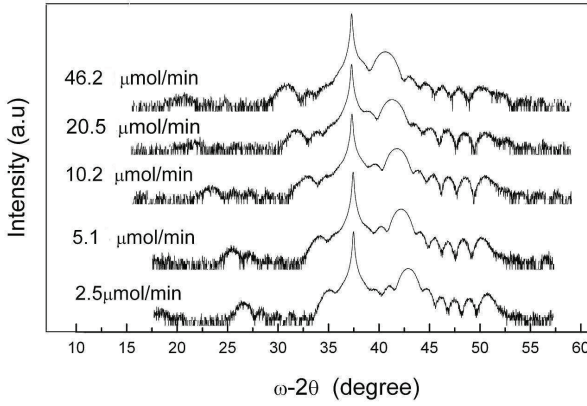
**Figure 6.16.** Temperature versus time profile during the growth process [ Publication VI].

Fig. 6.17 shows the HRXRD  $\omega - 2\theta$  scans for (002) reflection of five different samples with varying TMIn flows during the barrier growth. The sharper peak in the center with the highest intensity is from the GaN buffer layer. The broader peak on the right of the GaN peak comes from the InGaIn/InAlGaIn superlattice. The combined results from HRXRD scans and SIMS measurements show that the introduction of In into the barriers reduces the Al content in the barriers. The shifting of superlattice peak towards the GaN peak shows that there is a slight reduction in the tensile strain in the MQW stack with the increase of TMIn flow.

**Table 6.2.** In and Al composition in the barrier and corresponding precursor flows [ Publication VI].

TMIn flow*	TMAI flow*	In (%)	Al (%)	Growth rate**
2.5	51	0.6	16	0.11
5.1	51	0.7	16	0.11
10.3	51	1.1	15.5	0.10
20.5	51	1.3	14.5	0.09
46.2	51	1.6	13.0	0.08

\* $\mu\text{mol/min}$ , \*\*  $\text{nm/sec}$



**Figure 6.17.** HRXRD  $\omega - 2\theta$  scans for (0002) reflection of InGaN/InAlGaN MQWs with varying indium content in InAlGaN barriers [ Publication VI].

Fig. 6.18 shows the IQEs of the samples calculated from the normalized Arrhenius plots by performing temperature dependent PL measurements. The emission spectra were measured by varying the temperature from 10 to 300 K. The total luminescence intensity ratios from 15 to 300 K ( $\frac{I_{300}}{I_{15}}$ ) were used to estimate the IQE as the total integrated intensities at 10 K and 15 K were equal. It was assumed that non-radiative recombination was negligible at very low temperatures.

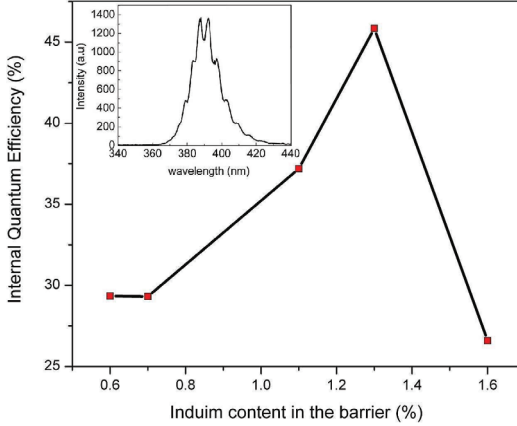


**Figure 6.18.** Internal quantum efficiencies (IQEs) with different barrier compositions [ Publication VI].

The results from our experiments indicate that the IQE increases with increasing In content until  $\sim 1.3\%$  and decreases rapidly at higher values. We believe that the increase of IQE is due to the reduction of tensile strain in the MQW stack. However, when the In content of the barriers exceeds 1.3 % the material quality deteriorates. Our previous results have shown

that InAlGa<sub>N</sub> barriers grown with 46  $\mu\text{mol}/\text{min}$  of TMIn flow have highly non uniform distribution of Al. The inset shows the room temperature PL spectrum of the sample with the highest IQE. The interference fringes in the PL spectrum appear from the multiple reflections suffered by the light generated in III-nitride layers grown on sapphire substrates [133]. The PL peak has a FWHM of 18 nm. The FWHM for the samples with the different TMIn flows were within the range of  $18\pm 2$  nm.



## 7. GaN LEDs and micro-display for a contact lens

GaN based LEDs can be used in novel technologies like miniaturized displays for applications in smart contact lenses [ Publication VII]. Contact lenses with biosensors capable of measuring eye movement, glucose concentration in the tear fluid, corneal temperature and blood oxygen levels have already been demonstrated [134]. A futuristic contact lens could be a fully functional computing device that may interact and share information with some external platforms (*e.g.*, mobile phones, tablets). The individual building blocks of such contact lenses may include a LED based pixel array, biosensors, focusing optics, an antenna and electric circuitry for power harvesting, radio communications and pixel control (Fig. 7.1).

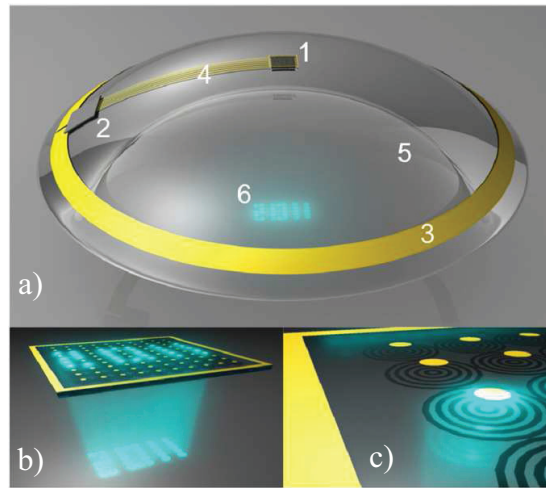


**Figure 7.1.** Conceptual rendition of a multi-pixel contact lens display. (a) A contact lens display comprising a multi-pixel LED chip (1), power-harvesting/control circuitry (2), antenna (3), and interconnects (4). These subsystems are encapsulated in a transparent polymer (5), creating a system to project virtual images (6) perceivable by the eye of the wearer. (b) LED chip with 100 pixels. LED active layers can be grown atop a transparent substrate. Emitted light travels through the substrate and is re-imaged using planar Fresnel lenses. (c) Magnified view with one pixel activated, showing Fresnel lenses opposite to each LED pixel [ Publication VII].

To implement the above mentioned concept LED display chips with single micro-pixel and 8 micro-pixels (circular and square shaped) were fabricated. This single-pixel contact lens display comprised of a LED, an antenna, an integrated circuit (IC) for power harvesting and LED control, and a polymer substrate with electrical interconnects. An external transmitting antenna was used to emit RF radiation that was collected by the on-lens antenna. The function of the integrated circuit was to rectify and store the energy, and regulate the duty cycle for the power to the LED at a frequency sufficiently high to give the appearance of continual light emission.

GaN based micro-LED was employed for the single pixel display module of the lens. A two-step technique was used to grow a GaN buffer layer on the sapphire substrate. This was followed by growth of a 2  $\mu\text{m}$  thick n-doped GaN layer at 1030  $^{\circ}\text{C}$ . A MQW stack consisting of five pairs of 3 nm thick InGaN (QWs) and 20 nm thick GaN barriers was grown on the n-doped GaN layer. InGaN growth was performed at 760  $^{\circ}\text{C}$  to ensure sufficient indium incorporation in the wells, whereas the GaN barriers were grown at higher temperatures to achieve acceptable surface morphology. A 50 nm GaN capping layer was grown on the QW stack before the temperature was increased to 970  $^{\circ}\text{C}$  to grow 250 nm of p-GaN. The capping layer prevents desorption of indium from the QWs during higher temperature steps. Finally the LED structure was annealed inside the MOVPE reactor for p-GaN activation. The schematics of the LED stack is shown in Fig. 7.2 .

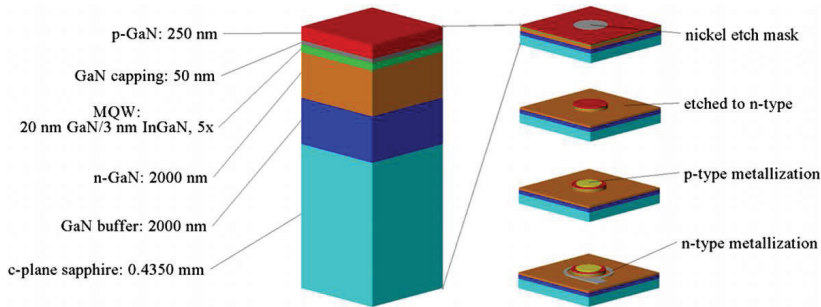


**Figure 7.2.** Schematic depicting the micro-LED growth stack (left) and post-growth fabrication process (right) [ Publication VII].

The process of forming electrical contacts required three lithography steps. Evaporation and lift-off procedure was utilized to cover the surface with required metals. Ni was used as an etch mask to define pixel size (diameter  $\sim 260 \mu\text{m}$ ) and shape. Chlorine-based plasma was used to etch

800 nm through the p-GaN and MQW stack to expose the n-GaN layer. A combination of Ni/Au/Ag/Au (5/5/70/200 nm) for p-type and Ni/Al/Au (20/860/200 nm) for n-type metal contacts were evaporated onto the GaN surfaces by using separate lithography steps. Finally, the wafers were thinned to 250  $\mu\text{m}$  by using lapping and grinding processes and diced into 750 x 750  $\mu\text{m}^2$  chips prior to assembly on the contact lens platform. The schematics of LED chips is shown in Fig. 7.2.

Micro-pixel LEDs were tested using an electrical probe station and a light collection system comprising an optical fiber, integrating sphere and photometer. Fig. 7.3 shows the LED pixel in off and on states, measured current–voltage characteristics, measured spectral output and measured electrical-to-optical power conversion efficiency.

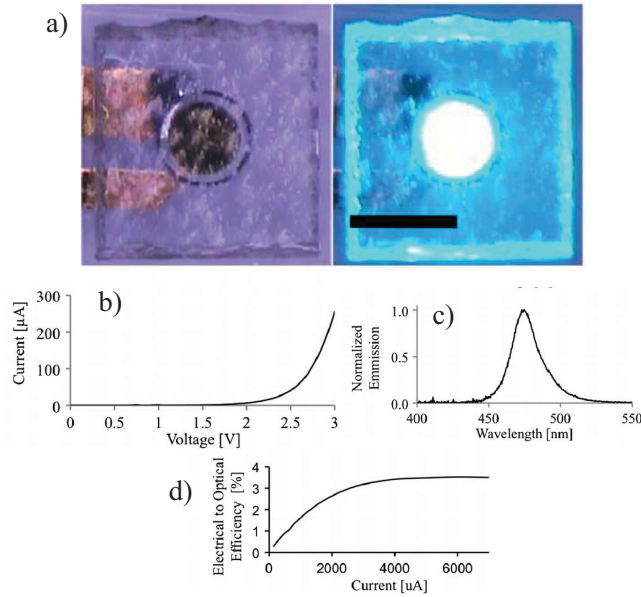


**Figure 7.3.** Optical micrographs as well as electrical and optical characteristics of the LED chip. (a) A top view of the  $\mu$ -pixel LED chip assembled onto a polymer template, taken looking through the sapphire substrate. The scale bar is 375  $\mu\text{m}$ . Upon application of a bias voltage (right), the micro-LED pixel emits light. (b) Measured current versus bias voltage. (c) Measured light emission spectrum. (d) Measured efficiency versus bias current for a 260  $\mu\text{m}$  circular pixel. Peak emission is at 475 nm (blue) while operating at 3.0 V [ Publication VII].

Self assembly process was used to place and connect the silicon microchip and micro-pixel LED onto the contact lens. Fig. 7.4a shows a complete functional lens with working components. A more detailed description of self assembly process for micro-components on plastic substrates is given by Stauth *et al.*, [135]. The contact lens system was tested in two steps.

First, the LED activation was tested using loop and horn antennas in free space. The micro-LED was visible when illuminated using horn antenna from a distance of 1 m. The second phase involved testing on rabbits. The testing of contact lens with active components including a single micro-pixel LED is shown in Fig. 7.4b. All in vivo studies were performed according to the guidelines of the National Institutes of Health for use of laboratory animals, and with the approval of the Institute of Animal Care and Use Committee of the University of Washington (Protocol UW4139-01).

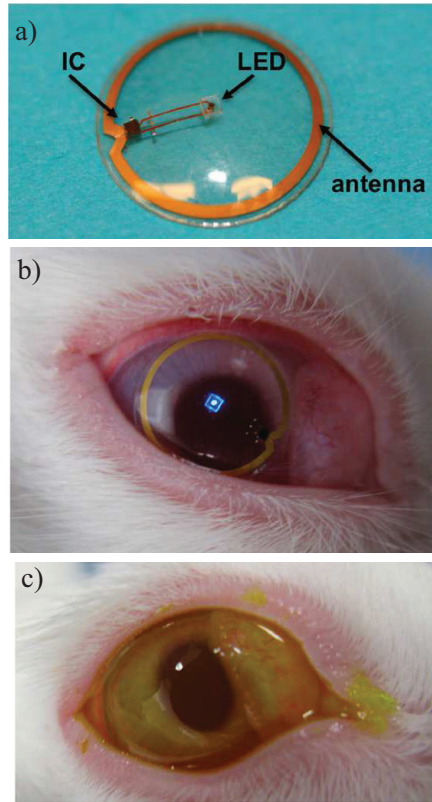


**Figure 7.4.** Testing the contact lens display on a live rabbit. (a) Photograph of a completed contact lens system. (b) The contact lens display is placed on the eye of a rabbit and powered by a dipole antenna, showing bright emission from the on-lens pixel. (c) Subsequent tests using fluorescein showed no corneal epithelial damage [ Publication VII].

Tests on a rabbit's eye showed activation of the LED from  $\sim 10$  cm with the horn antenna. The effect of wearing the contact lens display on the rabbit cornea was also evaluated. Additionally, topical fluorescein was applied to the corneal surface using a dropper and the eye was visually examined for potential corneal abrasion, thermal burn or corneal edema

as a result of in vivo testing. Such damage would result in corneal surface roughness, causing the fluorescein to accumulate. Fig. 7.4c demonstrates a healthy corneal epithelial layer after testing, showing no fluorescein streaks or cloudiness.

Our prototype device proves that an active lens system can be realized with the current technology. GaN based LEDs can certainly play an important role in this kind of futuristic micro-display system. Adding more pixels and colors to the display module could be the next target that might be demonstrated in the near future.



## 8. Summary

Fabrication and properties of GaN layers, III-N blue and near-UV light emitting structures and a novel application of GaN-based LEDs was investigated. The scope of this work was to improve the material quality of III-N layers, enhance light extraction efficiency and study new applications for nitride LEDs.

First, a novel method for improving the light extraction efficiency of LEDs was presented. This consists of patterning GaN on sapphire templates with hexagonal openings. The growth conditions for epitaxy were optimized to achieve coalescence of GaN surface along with the formation of embedded voids at the GaN-sapphire interface. It was found that the embedded voids change their shape if the diameter of the opening is varied while keeping every other parameter constant. The embedded void shape control from inclined ( $60^\circ$ ) to nearly vertical ( $85^\circ$ ) sidewalls was demonstrated. The GaN epi-layers with inclined void shape also showed an improved material quality. Threading dislocation bending was observed to increase as the inclination angle of the void sidewall decreased. The InGaN/GaN LED structures were grown to study the influence of GaN layers having embedded voids of different geometries. The LEDs with  $60^\circ$  sidewall voids showed almost 21 % improvement in the light output at 20 mA compared to the reference LEDs. This improvement in device performance was attributed to the improved material quality and more efficient light extraction from voids with the inclined sidewalls. Another method of light extraction by maskless roughening of the backside of sapphire substrate was also investigated. The chemical roughening of sapphire in hot acid seemed to significantly enhance the light extraction.

To improve the carrier confinement in near UV-emitters, the growth conditions and properties of quaternary InAlGaIn layers were investigated.

The layer quality for the InAlGaN layer was found to degrade for an indium content of more than 1.6 %. The optimized MQW stack with InAlGaN barrier showed an IQE of 45 % at 382 nm.

The operation of a contact lens display powered by a remote radio frequency transmitter was demonstrated in free space and on a live rabbit. GaN based micrometer-scale light sources can be integrated into a contact lens and operated on rabbit eyes. Although the display had only a single controllable pixel, the first proof-of-concept GaN LED micro display was demonstrated. The individual pixels can have any planar shape. GaN LED chips with 8 micro-pixels were also fabricated to carry out more elaborate tests.

Future research work could include the testing of green, blue and UV LED structures on GaN layers with optimized voids located at GaN-sapphire interface. It would also be interesting to perform a comprehensive study on the exact quantification of IQEs and EQEs for such LEDs with embedded voids. Another idea could be to fabricate LED structures on sub-micron openings on GaN templates. GaN template thickness could also be varied and its effect on the void formation is another interesting area to explore. As far as micro-LED displays are concerned, the possibilities are endless. The next logical step for micro-LEDs displays would be the fabrication of multiple pixel display to create an alphanumeric display and their integration with Fresnel lenses.

# Bibliography

- [1] R. Haitz and J. Y. Tsao, "Solid-state lighting," *Optik & Photonik*, vol. 6, no. 2, pp. 26–30, 2011.
- [2] B. Parviz, "For your eye only," *IEEE Spectrum*, vol. 46, no. 9, pp. 36–41, 2009.
- [3] A. Ferscha and S. Vogl, "Wearable displays for everyone!," *Pervasive Computing, IEEE*, vol. 9, no. 1, pp. 7–10, 2010.
- [4] V. Rawat, D. N. Zakharov, E. A. Stach, and T. D. Sands, "Pseudomorphic stabilization of rocksalt GaN in TiN/GaN multilayers and superlattices," *Phys. Rev. B*, vol. 80, pp. 024114–, July 2009.
- [5] S. Nakamura, S. Pearton, and G. Fasol, *The blue laser diode: the complete story*. Springer, 2000.
- [6] G. Ghione, *Semiconductor devices for high-speed optoelectronics*. Cambridge University Press, 2009.
- [7] J. Wu, "When group-III nitrides go infrared: New properties and perspectives," *J. Appl. Phys.*, vol. 106, pp. 011101–28, July 2009.
- [8] G. D. Chen, M. Smith, J. Y. Lin, H. X. Jiang, S.-H. Wei, M. A. Khan, and C. J. Sun, "Fundamental optical transitions in GaN," *Appl. Phys. Lett.*, vol. 68, pp. 2784–2786, May 1996.
- [9] M. D. McCluskey, C. G. Van de Walle, C. P. Master, L. T. Romano, and N. M. Johnson, "Large band gap bowing of InGaN alloys," *Appl. Phys. Lett.*, vol. 72, pp. 2725–2726, May 1998.
- [10] O. Katz, B. Meyler, U. Tisch, and J. Salzman, "Determination of band-gap bowing for AlGaIn alloys," *Phys. Status Solidi (a)*, vol. 188, no. 2, pp. 789–792, 2001.
- [11] M. Androulidaki, N. T. Pelekanos, K. Tsagaraki, E. Dimakis, E. Iliopoulos, A. Adikimenakis, E. Bellet-Amalric, D. Jalabert, and A. Georgakilas, "Energy gaps and bowing parameters of InAlGaIn ternary and quaternary alloys," *Phys. Status Solidi (c)*, vol. 3, no. 6, pp. 1866–1869, 2006.
- [12] A. Kazimirov, G. Scherb, J. Zegenhagen, T.-L. Lee, M. J. Bedzyk, M. K. Kelly, H. Angerer, and O. Ambacher, "Polarity determination of a GaN thin film on sapphire (0001) with x-ray standing waves," *J. Appl. Phys.*, vol. 84, pp. 1703–1705, Aug. 1998.

- [13] B. Daudin, J. L. Rouviere, and M. Arlery, "Polarity determination of GaN films by ion channeling and convergent beam electron diffraction," *Appl. Phys. Lett.*, vol. 69, pp. 2480–2482, Oct. 1996.
- [14] F. A. Ponce, D. P. Bour, W. T. Young, M. Saunders, and J. W. Steeds, "Determination of lattice polarity for growth of GaN bulk single crystals and epitaxial layers," *Appl. Phys. Lett.*, vol. 69, pp. 337–339, July 1996.
- [15] F. Bernardini, V. Fiorentini, and D. Vanderbilt, "Spontaneous polarization and piezoelectric constants of III-V nitrides," *Phys. Rev. B*, vol. 56, pp. R10024–R10027, Oct. 1997.
- [16] E. T. Yu, X. Z. Dang, P. M. Asbeck, S. S. Lau, and G. J. Sullivan, "Spontaneous and piezoelectric polarization effects in III-V nitride heterostructures," *J. Vac. Sci. Technol. B*, vol. 17, no. 4, pp. 1742–1749, 1999.
- [17] T. Paskova, D. Hanser, and K. Evans, "GaN substrates for III-nitride devices," *Proceedings of the IEEE*, vol. 98, no. 7, pp. 1324–1338, 2010.
- [18] M. Feneberg and K. Thonke, "Polarization fields of III-nitrides grown in different crystal orientations," *J. Phys.: Condens. Matter*, vol. 19, p. 403201, 2007.
- [19] T. Takeuchi, C. Wetzel, S. Yamaguchi, H. Sakai, H. Amano, I. Akasaki, Y. Kaneko, S. Nakagawa, Y. Yamaoka, and N. Yamada, "Determination of piezoelectric fields in strained GaInN quantum wells using the quantum-confined stark effect," *Appl. Phys. Lett.*, vol. 73, pp. 1691–1693, Sept. 1998.
- [20] A. Hangleiter, F. Hitzel, S. Lahmann, and U. Rossow, "Composition dependence of polarization fields in GaInN/GaN quantum wells," *Appl. Phys. Lett.*, vol. 83, pp. 1169–1171, Aug. 2003.
- [21] E. Schubert, *Light-emitting diodes (second edition)*. Cambridge University Press, 2nd edition ed., 2006.
- [22] S. Chichibu, T. Sota, K. Wada, and S. Nakamura, "Exciton localization in InGaN quantum well devices," *J. Vac. Sci. Technol. B*, vol. 16, pp. 2204–2214, July 1998.
- [23] J.-H. Ryou, P. Yoder, J. Liu, Z. Lochner, H. Kim, S. Choi, H. J. Kim, and R. Dupuis, "Control of quantum-confined stark effect in InGaN-based quantum wells," *IEEE Journal Selected Topics in Quantum Electronics*, vol. 15, no. 4, pp. 1080–1091, 2009.
- [24] S. Chichibu, A. Abare, M. Mack, M. Minsky, T. Deguchi, D. Cohen, P. Kozodoy, S. Fleischer, S. Keller, J. Speck, J. Bowers, E. Hu, U. Mishra, L. Coldren, S. DenBaars, K. Wada, T. Sota, and S. Nakamura, "Optical properties of InGaN quantum wells," *Mater. Sci. Eng., B*, vol. 59, pp. 298–306, May 1999.
- [25] H. Zhou, S. Chua, K. Zang, L. Wang, S. Tripathy, N. Yakovlev, and O. Thomas, "InGaN multiple quantum wells grown on ELO GaN templates and the optical properties characterization," *J. Cryst. Growth*, vol. 298, pp. 511–514, Jan. 2007.

- [26] V. Mymrin, K. Bulashevich, N. Podolskaya, and S. Karpov, "Bandgap engineering of electronic and optoelectronic devices on native AlN and GaN substrates: A modelling insight," *J. Cryst. Growth*, vol. 281, pp. 115–124, July 2005.
- [27] H. Morkoc, *Handbook of Nitride Semiconductors and Devices: Materials properties, physics and growth*. Wiley-VCH, 2008.
- [28] N. Grandjean, J. Massies, P. Vennegues, M. Laugt, and M. Leroux, "Epitaxial relationships between GaN and sapphire (0001) substrates," *Appl. Phys. Lett.*, vol. 70, pp. 643–645, Feb. 1997.
- [29] V. Lebedev, K. Tonisch, F. Niebelschutz, V. Cimalla, D. Cengher, I. Cimalla, C. Mauder, S. Hauguth, O. Ambacher, F. M. Morales, J. G. Lozano, and D. Gonzalez, "Coalescence aspects of III-nitride epitaxy," *J. Appl. Phys.*, vol. 101, pp. 054906–12, Mar. 2007.
- [30] M. Leszczynski, T. Suski, P. Perlin, H. Teisseyre, I. Grzegory, M. Bockowski, J. Jun, S. Porowski, and J. Major, "Lattice-constants, thermal-expansion and compressibility of gallium nitride," *J. Phys. D: Appl. Phys.*, vol. 28, no. 4A, pp. A149–A153, 1995.
- [31] L. J. Nasser N.M, Ye Zhi zhen and X. Y. bou, "GaN heteroepitaxial growth techniques," *J. Microwav. Optoelec.*, vol. 2, no. 4A, pp. 22–31, 2001.
- [32] S. Nakamura, M. Senoh, N. Iwasa, and S. ichi Nagahama, "High-brightness InGaN blue, green and yellow light-emitting diodes with quantum well structures," *Jpn. J. Appl. Phys.*, vol. 34, no. No. 7A, pp. L797–L799, 1995.
- [33] S. Nakamura, M. Senoh, S. ichi Nagahama, N. Iwasa, T. Yamada, T. Matsushita, H. Kiyoku, and Y. Sugimoto, "InGaN-based multi-quantum-well-structure laser diodes," *Jpn. J. Appl. Phys.*, vol. 35, no. No. 1B, pp. L74–L76, 1996.
- [34] A. Koukitu, N. Takahashi, and H. Seki, "Thermodynamic study on metalorganic vapor-phase epitaxial growth of group III nitrides," *Jpn. J. Appl. Phys.*, vol. 36, no. Part 2, No. 9A/B, pp. L1136–L1138, 1997.
- [35] J. J. Coleman, "Metalorganic chemical vapor deposition for optoelectronic devices," *Proceedings of the IEEE*, vol. 85, no. 11, pp. 1715–1729, 1997.
- [36] A. Koukitu, N. Takahashi, T. Taki, and H. Seki, "Thermodynamic analysis of the MOVPE growth of InGaN," *J. Cryst. Growth*, vol. 170, pp. 306–311, Jan. 1997.
- [37] S. S. Liu and D. A. Stevenson, "Growth kinetics and catalytic effects in the vapor phase epitaxy of gallium nitride," *J. Electrochem. Soc.*, vol. 125, pp. 1161–1169, July 1978.
- [38] *Technical manual of Thomas Swan Scientific Equipment Ltd.*, 2004.
- [39] H. P. Maruska and J. J. Tietjen, "The preparation and properties of vapor-deposited single-crystal-line GaN," *Appl. Phys. Lett.*, vol. 15, pp. 327–329, Nov. 1969.

- [40] H. Amano, N. Sawaki, I. Akasaki, and Y. Toyoda, "Metalorganic vapor phase epitaxial growth of a high quality GaN film using an AlN buffer layer," *Appl. Phys. Lett.*, vol. 48, pp. 353–355, Feb. 1986.
- [41] S. Nakamura, "GaN growth using GaN buffer layer," *Jpn. J. Appl. Phys.*, vol. 30, no. Part 2, No. 10A, pp. L1705–L1707, 1991.
- [42] S. Keller and S. P. DenBaars, "Metalorganic chemical vapor deposition of group III-nitrides: a discussion of critical issues," *J. Cryst. Growth*, vol. 248, pp. 479–486, Feb. 2003.
- [43] A. Hushur, M. H. Manghnani, and J. Narayan, "Raman studies of GaN/sapphire thin film heterostructures," *Journal of Applied Physics*, vol. 106, no. 5, p. 054317, 2009.
- [44] X. H. Wu, D. Kapolnek, E. J. Tarsa, B. Heying, S. Keller, B. P. Keller, U. K. Mishra, S. P. DenBaars, and J. S. Speck, "Nucleation layer evolution in metal-organic chemical vapor deposition grown GaN," *Applied Physics Letters*, vol. 68, no. 10, pp. 1371–1373, 1996.
- [45] Y.-K. Kuo, J.-Y. Chang, and M.-C. Tsai, "Enhancement in hole-injection efficiency of blue InGaN light-emitting diodes from reduced polarization by some specific designs for the electron blocking layer," *Opt. Lett.*, vol. 35, pp. 3285–3287, Oct. 2010.
- [46] T. G. Zhu, U. Chowdhury, J. C. Denyszyn, M. M. Wong, and R. D. Dupuis, "AlGaIn/AlGaIn UV light-emitting diodes grown on sapphire by metalorganic chemical vapor deposition," *J. Cryst. Growth*, vol. 248, pp. 548–551, Feb. 2003.
- [47] S. Grzanka, G. Franssen, G. Targowski, K. Krowicki, T. Suski, R. Czernecki, P. Perlin, and M. Leszczynski, "Role of the electron blocking layer in the low-temperature collapse of electroluminescence in nitride light-emitting diodes," *Appl. Phys. Lett.*, vol. 90, pp. 103507–3, Mar. 2007.
- [48] R. Dahal, B. Pantha, J. Li, J. Y. Lin, and H. X. Jiang, "InGaIn/GaN multiple quantum well solar cells with long operating wavelengths," *Appl. Phys. Lett.*, vol. 94, pp. 063505–3, Feb. 2009.
- [49] S. Bedair, F. McIntosh, J. Roberts, E. Piner, K. Boutros, and N. El-Masry, "Growth and characterization of In-based nitride compounds," *J. Cryst. Growth*, vol. 178, pp. 32–44, June 1997.
- [50] C. Hums, A. Gadanez, A. Dadgar, J. Bläsing, P. Lorenz, S. Krischok, F. Bertram, A. Franke, J. A. Schaefer, J. Christen, and A. Krost, "AlInN/GaN based multi quantum well structures-growth and optical properties," *Phys. Status Solidi (c)*, vol. 6, no. S2, pp. S451–S454, 2009.
- [51] A. R. Smith, R. M. Feenstra, D. W. Greve, M. S. Shin, M. Skowronski, J. Neugebauer, and J. E. Northrup, "Reconstructions of GaN(0001) and (0001-bar) surfaces: Ga-rich metallic structures," *J. Vac. Sci. Technol. B*, vol. 16, pp. 2242–2249, July 1998.
- [52] O. Ambacher, "Growth and applications of group III-nitrides," *J. Phys. D: Appl. Phys.*, vol. 31, no. 20, pp. 2653–2710, 1998.

- [53] E. L. Piner, M. K. Behbehani, N. A. El-Masry, F. G. McIntosh, J. C. Roberts, K. S. Boutros, and S. M. Bedair, "Effect of hydrogen on the indium incorporation in InGaN epitaxial films," *Appl. Phys. Lett.*, vol. 70, pp. 461–463, Jan. 1997.
- [54] T. G. Mihopoulos, V. Gupta, and K. F. Jensen, "A reaction-transport model for AlGaIn MOVPE growth," *J. Cryst. Growth*, vol. 195, pp. 733–739, Dec. 1998.
- [55] A. Lobanova, K. Mazaev, R. Talalaev, M. Leys, S. Boeykens, K. Cheng, and S. Degroote, "Effect of V/III ratio in AlN and AlGaIn MOVPE," *J. Cryst. Growth*, vol. 287, pp. 601–604, Jan. 2006.
- [56] M. E. Coltrin, J. Randall Creighton, and C. C. Mitchell, "Modeling the parasitic chemical reactions of AlGaIn organometallic vapor-phase epitaxy," *J. Cryst. Growth*, vol. 287, pp. 566–571, Jan. 2006.
- [57] J. Lee, H. Cho, D. Hays, C. Abernathy, S. Pearton, R. Shul, G. Vawter, and J. Han, "Dry etching of GaN and related materials: comparison of techniques," *IEEE J. Sel. Topics in Quantum Electron.*, vol. 4, pp. 557 – 563, may/jun 1998.
- [58] I. Adesida, C. Youtsey, A. T. Ping, F. Khan, L. T. Romano, and G. Bulman, "Dry and wet etching for group III-nitrides," *MRS Internet J. Nitride Semicond. Res.*, vol. 4S1-4S11, pp. G1.4 –563, 1999.
- [59] J.-M. Lee, K.-M. Chang, I.-H. Lee, and S.-J. Park, "Highly selective dry etching of III nitrides using an inductively coupled Cl<sub>2</sub>/Ar/O<sub>2</sub> plasma," *J. Vac. Sci. Technol. B*, vol. 18, pp. 1409–1411, May 2000.
- [60] K. Remashan, S. J. Chua, A. Ramam, S. Prakash, and W. Liu, "Inductively coupled plasma etching of GaN using BCl<sub>3</sub>/Cl<sub>2</sub> chemistry and photoluminescence studies of the etched samples," *Semicond. Sci. Technol.*, vol. 15, no. 4, pp. 386 –389, 2000.
- [61] M. E. Ryan, A. C. Camacho, and J. K. Bhardwaj, "High etch rate gallium nitride processing using an inductively coupled plasma source," *Phys. Status Solidi (a)*, vol. 176, no. 1, pp. 743–746, 1999.
- [62] K.-C. Shen, D.-S. Wu, C.-C. Shen, S.-L. Ou, and R.-H. Horng, "Surface modification on wet-etched patterned sapphire substrates using plasma treatments for improved GaN crystal quality and LED performance," *J. Electrochem. Soc.*, vol. 158, pp. H988–H993, Oct. 2011.
- [63] Y. Hsu, S. Chang, Y. Su, J. Sheu, C. Kuo, C. Chang, and S. Shei, "ICP etching of sapphire substrates," *Optical Materials*, vol. 27, pp. 1171–1174, Mar. 2005.
- [64] K. Birdi, *Scanning probe microscopes: applications in science and technology*. CRC Press, 2003.
- [65] D. Brandon and W. Kaplan, *Microstructural characterization of materials*. John Wiley, 2008.
- [66] L. Lu, B. Shen, F. J. Xu, J. Xu, B. Gao, Z. J. Yang, G. Y. Zhang, X. P. Zhang, J. Xu, and D. P. Yu, "Morphology of threading dislocations in high-resistivity GaN films observed by transmission electron microscopy," *J. Appl. Phys.*, vol. 102, pp. 033510–5, Aug. 2007.

- [67] B. Heying, X. H. Wu, S. Keller, Y. Li, D. Kapolnek, B. P. Keller, S. P. Den-Baars, and J. S. Speck, "Role of threading dislocation structure on the x-ray diffraction peak widths in epitaxial GaN films," *Appl. Phys. Lett.*, vol. 68, pp. 643–645, Jan. 1996.
- [68] H. Heinke, V. Kirchner, S. Einfeldt, and D. Hommel, "Analysis of the defect structure of epitaxial GaN," *Phys. Status Solidi (a)*, vol. 176, no. 1, pp. 391–395, 1999.
- [69] P. Fewster, *X-Ray Scattering from Semiconductors*. Imperial College Press, 2000.
- [70] S. Sintonen, S. Suihkonen, O. Svensk, P. T. Törmä, M. Ali, M. Sopanen, and H. Lipsanen, "Characterization of InGaN/GaN and AlGaIn/GaN superlattices by X-ray diffraction and X-ray reflectivity measurements," *Phys. Status Solidi (c)*, vol. 7, pp. 1790–1793, June 2010.
- [71] M. Köhler and W. Fritzsche, *Nanotechnology: An Introduction to Nanostructuring Techniques*. John Wiley & Sons, 2008.
- [72] A. Bhattacharyya, T. D. Moustakas, L. Zhou, D. J. Smith, and W. Hug, "Deep ultraviolet emitting AlGaIn quantum wells with high internal quantum efficiency," *Appl. Phys. Lett.*, vol. 94, pp. 181907–3, May 2009.
- [73] J. Son, S. Lee, T. Sakong, H. Paek, O. Nam, Y. Park, J. Hwang, J. Kim, and Y. Cho, "Enhanced optical properties of InGaIn MQWs with InGaIn underlying layers," *J. Cryst. Growth*, vol. 287, pp. 558–561, Jan. 2006.
- [74] A. Khan, K. Balakrishnan, and T. Katona, "Ultraviolet light-emitting diodes based on group three nitrides," *Nat Photon*, vol. 2, pp. 77–84, Feb. 2008.
- [75] A. Osinsky, S. Gangopadhyay, B. W. Lim, M. Z. Anwar, M. A. Khan, D. V. Kuksenkov, and H. Temkin, "Schottky barrier photodetectors based on Al-GaN," *Appl. Phys. Lett.*, vol. 72, pp. 742–744, Feb. 1998.
- [76] I. Akasaki, "The evolution of group III nitride semiconductors: Seeking blue light emission," *Mater. Sci. Eng., B*, vol. 74, pp. 101–106, May 2000.
- [77] I. Akasaki, "Key inventions in the history of nitride-based blue LED and LD," *J. Cryst. Growth*, vol. 300, pp. 2–10, Mar. 2007.
- [78] S. Nakamura, T. Mukai, M. Senoh, and N. Iwasa, "Thermal annealing effects on p-type Mg-doped GaN films," *Jpn. J. Appl. Phys.*, vol. 31, no. Part 2, No. 2B, pp. L139–L142, 1992.
- [79] S. Nakamura, N. Iwasa, M. Senoh, and T. Mukai, "Hole compensation mechanism of p-type GaN films," *Jpn. J. Appl. Phys.*, vol. 31, no. Part 1, No. 5A, pp. 1258–1266, 1992.
- [80] S. Y. Karpov, "Modeling of III-nitride light-emitting diodes: progress, problems, and perspectives," *Proc. SPIE*, vol. 7939, pp. 79391C–12, Feb. 2011.
- [81] J. Tsao, "Solid-state lighting: lamps, chips, and materials for tomorrow," *IEEE Circuit. Devic.*, vol. 20, pp. 28 – 37, may-june 2004.

- [82] Y. Yang, X. A. Cao, and C. H. Yan, "Rapid efficiency roll-off in high-quality green light-emitting diodes on freestanding GaN substrates," *Appl. Phys. Lett.*, vol. 94, pp. 041117–3, Jan. 2009.
- [83] C. G. Van de Walle, C. Stampfl, and J. Neugebauer, "Theory of doping and defects in III-V nitrides," *Journal of Crystal Growth*, vol. 189–190, pp. 505–510, June 1998.
- [84] J. K. Sheu and G. C. Chi, "The doping process and dopant characteristics of GaN," *J. Phys.: Condens. Matter*, vol. 14, no. 22, pp. R657–R702, 2002.
- [85] K. Kyhm and R. Taylor, "Dynamics of localized carriers in InGaN multi-quantum wells," *J. Korean Phys. Soc.*, vol. 49, no. 2, pp. 538–541, 2006.
- [86] G. Wu and S. Chen, "Blue InGaN/GaN light-emitting diodes using Mg-doped AlGaIn electron-blocking barriers," *J. Korean Phys. Soc.*, vol. 52, no. 5, pp. 1570–1574, 2008.
- [87] O. Svensk, P. Törmä, S. Suihkonen, M. Ali, H. Lipsanen, M. Sopanen, M. Odnoblyudov, and V. Bougrov, "Enhanced electroluminescence in 405 nm InGaN/GaN LEDs by optimized electron blocking layer," *J. Cryst. Growth*, vol. 310, pp. 5154–5157, Nov. 2008.
- [88] A. Knauer, V. Kueller, S. Einfeldt, V. Hoffmann, T. Kolbe, J.-R. van Look, J. Piprek, M. Weyers, and M. Kneissl, "Influence of the barrier composition on the light output of InGaN multiple-quantum-well ultraviolet light emitting diodes," *Proc. SPIE*, vol. 6797, pp. 67970X–6, 2007.
- [89] S. Kukushkin, A. Osipov, V. Bessolov, B. Medvedev, V. Nevolin, and K. Tcarik, "Substrates for epitaxy of gallium nitride: New materials and techniques," *J. Korean Phys. Soc.*, vol. 17, pp. 1–32, 2008.
- [90] C. R. Miskys, M. K. Kelly, O. Ambacher, and M. Stutzmann, "Freestanding GaN-substrates and devices," *Phys. Status Solidi (c)*, vol. 0, no. 6, pp. 1627–1650, 2003.
- [91] J. Piprek, "Efficiency droop in nitride-based light-emitting diodes," *Phys. Status Solidi (a)*, vol. 207, no. 10, pp. 2217–2225, 2010.
- [92] E. Kioupakis, P. Rinke, K. T. Delaney, and C. G. Van de Walle, "Indirect auger recombination as a cause of efficiency droop in nitride light-emitting diodes," *Appl. Phys. Lett.*, vol. 98, pp. 161107–3, Apr. 2011.
- [93] S. Pimputkar, J. S. Speck, S. P. DenBaars, and S. Nakamura, "Prospects for LED lighting," *Nat Photon*, vol. 3, pp. 180–182, Apr. 2009.
- [94] M. F. Schubert, J. Xu, J. K. Kim, E. F. Schubert, M. H. Kim, S. Yoon, S. M. Lee, C. Sone, T. Sakong, and Y. Park, "Polarization-matched GaInN/AlGaInN multi-quantum-well light-emitting diodes with reduced efficiency droop," *Appl. Phys. Lett.*, vol. 93, pp. 041102–3, July 2008.
- [95] Y.-L. Li, Y.-R. Huang, and Y.-H. Lai, "Investigation of efficiency droop behaviors of InGaN/GaN multiple-quantum-well leds with various well thicknesses," *IEEE J. Sel. Topics in Quantum Electron.*, vol. 15, pp. 1128–1131, july-aug. 2009.

- [96] J.-Y. Kim, M.-K. Kwon, J.-P. Kim, and S.-J. Park, "Enhanced light extraction from triangular GaN-based light-emitting diodes," *Photonics Technology Letters, IEEE*, vol. 19, pp. 1865–1867, dec.1, 2007.
- [97] T. Fujii, Y. Gao, R. Sharma, E. L. Hu, S. P. DenBaars, and S. Nakamura, "Increase in the extraction efficiency of GaN-based light-emitting diodes via surface roughening," *Appl. Phys. Lett.*, vol. 84, pp. 855–857, Feb. 2004.
- [98] O. B. Shchekin, J. E. Epler, T. A. Trottier, T. Margalith, D. A. Steigerwald, M. O. Holcomb, P. S. Martin, and M. R. Krames, "High performance thin-film flip-chip InGaN/GaN light-emitting diodes," *Appl. Phys. Lett.*, vol. 89, pp. 071109–3, Aug. 2006.
- [99] S.-M. Pan, R.-C. Tu, Y.-M. Fan, R.-C. Yeh, and J.-T. Hsu, "Improvement of InGaN-GaN light-emitting diodes with surface-textured ITO transparent ohmic contacts," *Photonics Technology Letters, IEEE*, vol. 15, no. 5, pp. 649–651, 2003.
- [100] P. Tsai, W. Chen, Y. Su, and C. Huang, "Enhanced light output of ingan leds with a roughened p-GaN surface using different TMGa flow rates in p-AlGaIn layer," *Applied Surface Science*, vol. 256, pp. 6694–6698, Oct. 2010.
- [101] K. McGroddy, A. David, E. Matioli, M. Iza, S. Nakamura, S. DenBaars, J. S. Speck, C. Weisbuch, and E. L. Hu, "Directional emission control and increased light extraction in GaN photonic crystal light emitting diodes," *Appl. Phys. Lett.*, vol. 93, pp. 103502–3, Oct. 2008.
- [102] C.-H. Chan, C.-H. Hou, S.-Z. Tseng, T.-J. Chen, H.-T. Chien, F.-L. Hsiao, C.-C. Lee, Y.-L. Tsai, and C.-C. Chen, "Improved output power of GaN-based light-emitting diodes grown on a nanopatterned sapphire substrate," *Appl. Phys. Lett.*, vol. 95, pp. 011110–3, July 2009.
- [103] D. S. Kuo, S. J. Chang, C. F. Shen, T. C. Ko, T. K. Ko, and S. J. Hon, "Nitride-based LEDs with oblique sidewalls and a light guiding structure," *Semiconductor Science and Technology*, vol. 25, no. 5, pp. –055010, 2010.
- [104] Y.-C. Huang, C.-F. Lin, S.-H. Chen, J.-J. Dai, G.-M. Wang, K.-P. Huang, K.-T. Chen, and Y.-H. Hsu, "InGaIn-based light-emitting diodes with an embedded conical air-voids structure," *Opt. Express*, vol. 19, pp. A57–A63, Jan. 2011.
- [105] T.-Y. Tang, W.-Y. Shiao, C.-H. Lin, K.-C. Shen, J.-J. Huang, S.-Y. Ting, T.-C. Liu, C. C. Yang, C.-L. Yao, J.-H. Yeh, T.-C. Hsu, W.-C. Chen, H.-C. Hsu, and L.-C. Chen, "Coalescence overgrowth of GaN nanocolumns on sapphire with patterned metal organic vapor phase epitaxy," *J. Appl. Phys.*, vol. 105, pp. 023501–8, Jan. 2009.
- [106] R. Colby, Z. Liang, I. H. Wildeson, D. A. Ewoldt, T. D. Sands, R. E. Garcia, and E. A. Stach, "Dislocation filtering in GaN nanostructures," *Nano Lett.*, vol. 10, pp. 1568–1573, Apr. 2010.
- [107] Y.-S. Chen, W.-Y. Shiao, T.-Y. Tang, W.-M. Chang, C.-H. Liao, C.-H. Lin, K.-C. Shen, C. C. Yang, M.-C. Hsu, J.-H. Yeh, and T.-C. Hsu, "Threading dislocation evolution in patterned GaN nanocolumn growth and coalescence overgrowth," *J. Appl. Phys.*, vol. 106, pp. 023521–6, July 2009.

- [108] C. H. Chiu, H. H. Yen, C. L. Chao, Z. Y. Li, P. Yu, H. C. Kuo, T. C. Lu, S. C. Wang, K. M. Lau, and S. J. Cheng, "Nanoscale epitaxial lateral overgrowth of GaN-based light-emitting diodes on a SiO<sub>2</sub> nanorod-array patterned sapphire template," *Appl. Phys. Lett.*, vol. 93, pp. 081108–3, Aug. 2008.
- [109] Z. Liliental-Weber, X. Ni, and H. Morkoc, "Structural perfection of laterally overgrown GaN layers grown in polar- and non-polar directions," *J. Mater. Sci.: Mater. Electron.*, vol. 19, pp. 815–820, 2008.
- [110] S. D. Hersee, X. Y. Sun, X. Wang, M. N. Fairchild, J. Liang, and J. Xu, "Nanoheteroepitaxial growth of GaN on Si nanopillar arrays," *J. Appl. Phys.*, vol. 97, pp. 124308–4, June 2005.
- [111] J.-J. Dai, C.-F. Lin, G.-M. Wang, and M.-S. Lin, "Enhanced the light extraction efficiency of an InGaN light emitting diodes with an embedded rhombus-like air-void structure," *Appl. Phys. Expr.*, vol. 3, no. 7, pp. 071002(1)–071002(3), 2010.
- [112] C.-F. Lin, J.-J. Dai, M.-S. Lin, K.-T. Chen, W.-C. Huang, C.-M. Lin, R.-H. Jiang, and Y.-C. Huang, "An AlN sacrificial buffer layer inserted into the GaN/patterned sapphire substrate for a chemical lift-off process," *Appl. Phys. Expr.*, vol. 3, no. 3, pp. 031001(1)–031001(3), 2010.
- [113] S. Bohyama, H. Miyake, K. Hiramatsu, Y. Tsuchida, and T. Maeda, "Freestanding GaN substrate by advanced facet-controlled epitaxial lateral overgrowth technique with masking side facets," *Jpn. J. Appl. Phys.*, vol. 44, no. 1, pp. L24–L26, 2005.
- [114] S. E. Bennett, "Dislocations and their reduction in GaN," *Mater. Sci. Technol.*, vol. 26, no. 9, pp. 1017–1028, 2010.
- [115] B. Beaumont, P. Vennegues, and P. Gibart, "Epitaxial lateral overgrowth of GaN," *Phys. Status Solidi (b)*, vol. 227, no. 1, pp. 1–43, 2001.
- [116] S. Gradecak, P. Stadelmann, V. Wagner, and M. Ilegems, "Bending of dislocations in GaN during epitaxial lateral overgrowth," *Appl. Phys. Lett.*, vol. 85, pp. 4648–4650, Nov. 2004.
- [117] H. J. Oh, S. W. Rhee, and I. S. Kang, "Simulation of CVD process by boundary integral technique," *J. Electrochem. Soc.*, vol. 139, pp. 1714–1720, June 1992.
- [118] T. Zheleva, S. Smith, D. Thomson, K. Linthicum, P. Rajagopal, and R. Davis, "Pendeo-epitaxy: A new approach for lateral growth of gallium nitride films," *J. Electron. Mater.*, vol. 28, pp. L5–L8, 1999.
- [119] K. Hiramatsu, "Epitaxial lateral overgrowth techniques used in group III nitride epitaxy," *Growth Lakeland*, vol. 13, no. 32, pp. 6961–6975, 2001.
- [120] X. Y. Sun, R. Bommen, D. Burckel, A. Frauenglass, M. N. Fairchild, S. R. J. Brueck, G. A. Garrett, M. Wraback, and S. D. Hersee, "Defect reduction mechanisms in the nanoheteroepitaxy of GaN on SiC," *J. Appl. Phys.*, vol. 95, pp. 1450–1454, Feb. 2004.

- [121] P. Dong Jun, L. Jeong Young, C. Hyung Koun, H. Chang Hee, and C. Hung Seob, "Dislocation reduction in GaN epilayers by maskless pendeo-epitaxy process," *Journal Of The Korean Physical Society*, vol. 45, no. 5, pp. 1253–1256, 2004.
- [122] R. Datta and C. J. Humphreys, "Mechanisms of bending of threading dislocations in MOVPE-grown GaN on (0001) sapphire," *Phys. Status Solidi (c)*, vol. 3, no. 6, pp. 1750–1753, 2006.
- [123] Y.-J. Chen, C.-H. Kuo, C.-J. Tun, S.-C. Hsu, Y.-J. Cheng, and C.-Y. Liu, "Fabrication of high-power InGaN-based light-emitting diode chips on pyramidally patterned sapphire substrate," *Japanese Journal of Applied Physics*, vol. 49, no. 2, p. 020201, 2010.
- [124] F. Dwikusuma, D. Saulys, and T. F. Kuech, "Study on sapphire surface preparation for iii-nitride heteroepitaxial growth by chemical treatments," *Journal of The Electrochemical Society*, vol. 149, pp. G603–G608, Jan. 2002.
- [125] H. Lin, C. L. X. Chen, Y.J.and Chang, C. Kuo, S. Hsu, and C. Liu, "Characterization study of GaN-based epitaxial layer and light-emitting diode on nature-patterned sapphire substrate," *Journal of Materials Research*, vol. 27, pp. 971–977, 2012.
- [126] S.-J. Chang, W. Chen, S. Shei, C. Kuo, T. Ko, C. Shen, J. Tsai, W.-C. Lai, J.-K. Sheu, and A. Lin, "High-brightness InGaN/GaN power flip-chip LEDs," *J. Light. Tech.*, vol. 27, no. 12, pp. 1985–1989, 2009.
- [127] H.-G. Chen, N.-F. Hsu, J.-T. Chu, H.-H. Yao, T.-C. Lu, H.-C. Kuo, and S.-C. Wang, "Strong ultraviolet emission from InGaN/AlGaN multiple quantum well grown by multi-step process," *Jpn. J. Appl. Phys.*, vol. 46, no. 4B, pp. 2574–2577, 2007.
- [128] Y. Sakai and T. Egawa, "Metal-organic chemical vapor deposition growth and characterization of InAlGaN multiple quantum wells," *Jpn. J. Appl. Phys.*, vol. 48, no. 7, p. 071001, 2009.
- [129] S.-H. Baek, J.-O. Kim, M.-K. Kwon, I.-K. Park, S.-I. Na, J.-Y. Kim, B. Kim, and S.-J. Park, "Enhanced carrier confinement in AlInGaN-InGaN quantum wells in near ultraviolet light-emitting diodes," *IEEE Photon. Technol. Lett.*, vol. 18, pp. 1276–1278, june 2006.
- [130] S. Zhou, M. Wu, S. Yao, J. Liu, and H. Yang, "Chemical composition and elastic strain in AlInGaN quaternary films," *Thin Solid Films*, vol. 515, pp. 1429–1432, Dec. 2006.
- [131] H. Hirayama, "Quaternary InAlGaN-based high-efficiency ultraviolet light-emitting diodes," *J. Appl. Phys.*, vol. 97, pp. 091101–19, May 2005.
- [132] A. Allerman, M. Crawford, A. Fischer, K. Bogart, S. Lee, D. Follstaedt, P. Provencio, and D. Koleske, "Growth and design of deep-UV light emitting diodes using AlGaN alloys," *J. Cryst. Growth*, vol. 272, pp. 227–241, Dec. 2004.
- [133] E. Namvar and M. Fattahi, "Interference effects on the photoluminescence spectrum of GaN/InGaN single quantum well structures," *J. Lumin.*, vol. 128, pp. 155–160, Jan. 2008.

- [134] M. X. Chu, K. Miyajima, D. Takahashi, T. Arakawa, K. Sano, S.-i. Sawada, H. Kudo, Y. Iwasaki, K. Akiyoshi, M. Mochizuki, and K. Mitsubayashi, "Soft contact lens biosensor for in situ monitoring of tear glucose as non-invasive blood sugar assessment," *Talanta*, vol. 83, pp. 960–965, Jan. 2011.
- [135] S. A. Stauth and B. A. Parviz, "Self-assembled single-crystal silicon circuits on plastic," *Proc. Natl. Acad. Sci. U. S. A.*, vol. 103, pp. 13922–13927, Sept. 2006.







ISBN 978-952-60-4845-1  
ISBN 978-952-60-4846-8 (pdf)  
ISSN-L 1799-4934  
ISSN 1799-4934  
ISSN 1799-4942 (pdf)

**Aalto University**  
**School of Electrical Engineering**  
**Department of Micro- and Nanosciences**  
[www.aalto.fi](http://www.aalto.fi)

**BUSINESS +  
ECONOMY**

**ART +  
DESIGN +  
ARCHITECTURE**

**SCIENCE +  
TECHNOLOGY**

**CROSSOVER**

**DOCTORAL  
DISSERTATIONS**